Concept development, floating bridge E39 Bjørnafjorden

Appendix E – Enclosure 1

Tower Load Coefficients during construction

Tower Load Coefficient

Code: NS-EN-1991-1-4:2005 §7.6

Assumptions:

- Wind perpendicular to one side of the cross section
- No end effects includled
- Drag load shall be calculated based on b, length facing the wind
- Lift based on worst in +/- 10 Deg range around perpendicular.
- Lift load shall be calculated based on d, length parallel to the wind
- for camfered cross sections r=camfer

Definitions:

$$f_D := \frac{1}{2}\cdot\rho\cdot C_D\cdot b\cdot V^2$$

$$f_L := \frac{1}{2}\cdot\rho\cdot C_L\cdot d\cdot V^2$$

Corner effects:

$$\Psi_r(\beta) := \begin{cases} \dfrac{(0.5-1.0)\cdot\beta}{0.2} + 1.0 & \text{if } \beta \le 0.2 \\ 0.5 & \text{otherwise} \end{cases}$$

Drag coefficient:

Formulaes

Drag base value is referenced to: α = d/b
Redcution factor for rounded corner: β = r/b

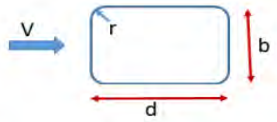

Base value:

$$f_{c0}(\alpha) := \begin{cases} 2.0 & \text{if } \alpha \le 0.2 \\ \left[\dfrac{(2.4-2.0)\cdot(\alpha-0.2)}{(0.7-0.2)} + 2.0\right] & \text{if } (\alpha \le 0.7 \wedge \alpha > 0.2) \\ \left[\dfrac{(1.0-2.4)\cdot(\alpha-0.7)}{(5.0-0.7)} + 2.4\right] & \text{if } (\alpha \le 5.0 \wedge \alpha > 0.7) \\ \left[\dfrac{(0.9-1.0)\cdot(\alpha-5.0)}{(10.0-5.0)} + 1.0\right] & \text{if } (\alpha \le 10.0 \wedge \alpha > 5.0) \\ 0.9 & \text{otherwise} \end{cases}$$

Shielding effects (from Chacao tests)

Downwind leg within +/- 20deg of upwind: Cd_downwind = 0.7*Cd_upwind

Derivatives (from Chacao tests):

Valid in the range alpha:[0.65,1.5]. Outside this the last value is used.

Single leg factors:

				Wind perpendicular to alignment								Wind along alignment						
Section No	b	d	r	α=d/b	β=r/b	fc0(α)	ψ(β)	Upwind Cd=fc0*ψ	Downwind Cd_downW	CL(α)	Cl'(α)	Cd'(α)	β=r/d	fc0(1/α)	ψ(β)	Cd=fc0*ψ	CL(1/α)	Cl'(1/α)	Cd'(1/α)
[]	[m]	[m]	[m]	[]	[]	[]	[]	[]	[]	[]	[1/rad]	[1/rad]	[]	[]	[]	[]	[]	[1/rad]	[1/rad]
1	12,000	7,000	0,60	0,583	0,050	2,307	0,875	2,018	1,413	0,500	2,800	3,500	0,086	2,070	0,786	1,626	0,300	3,500	1,420
2	11,895	6,942	0,60	0,584	0,050	2,307	0,874	2,016	1,411	0,500	2,800	3,500	0,086	2,070	0,784	1,623	0,300	3,500	1,420
3	11,790	6,885	0,60	0,584	0,051	2,307	0,873	2,014	1,410	0,500	2,800	3,500	0,087	2,070	0,782	1,619	0,300	3,500	1,420
4	11,685	6,827	0,60	0,584	0,051	2,307	0,872	2,011	1,408	0,500	2,800	3,500	0,088	2,071	0,780	1,616	0,300	3,500	1,420
5	11,579	6,769	0,60	0,585	0,052	2,308	0,870	2,009	1,406	0,500	2,800	3,500	0,089	2,071	0,778	1,612	0,300	3,500	1,420
6	11,474	6,712	0,60	0,585	0,052	2,308	0,869	2,006	1,404	0,500	2,800	3,500	0,089	2,071	0,777	1,608	0,300	3,500	1,420
7	11,369	6,654	0,60	0,585	0,053	2,308	0,868	2,004	1,403	0,500	2,800	3,500	0,090	2,072	0,775	1,605	0,300	3,500	1,420
8	11,264	6,596	0,60	0,586	0,053	2,308	0,867	2,001	1,401	0,500	2,800	3,500	0,091	2,072	0,773	1,601	0,300	3,500	1,420
9	11,159	6,539	0,60	0,586	0,054	2,309	0,866	1,998	1,399	0,500	2,800	3,500	0,092	2,072	0,771	1,597	0,300	3,500	1,420
10	11,054	6,481	0,60	0,586	0,054	2,309	0,864	1,996	1,397	0,500	2,800	3,500	0,093	2,073	0,769	1,593	0,300	3,500	1,420
11	10,948	6,423	0,60	0,587	0,055	2,309	0,863	1,993	1,395	0,500	2,800	3,500	0,093	2,073	0,766	1,589	0,300	3,500	1,420
12	10,890	6,392	0,60	0,587	0,055	2,310	0,862	1,991	1,394	0,500	2,800	3,500	0,094	2,073	0,765	1,587	0,300	3,500	1,420
13	10,768	6,324	0,60	0,587	0,056	2,310	0,861	1,988	1,392	0,500	2,800	3,500	0,095	2,074	0,763	1,582	0,300	3,500	1,420
14	10,646	6,257	0,60	0,588	0,056	2,310	0,859	1,985	1,389	0,500	2,800	3,500	0,096	2,074	0,760	1,577	0,300	3,500	1,420
15	10,523	6,190	0,60	0,588	0,057	2,311	0,857	1,981	1,387	0,500	2,800	3,500	0,097	2,074	0,758	1,572	0,300	3,500	1,420
16	10,401	6,123	0,60	0,589	0,058	2,311	0,856	1,978	1,384	0,500	2,800	3,500	0,098	2,075	0,755	1,567	0,300	3,500	1,420

AAS-JAKOBSEN COWI Multiconsult

JOHS HOLT AkerSolutions entail NGI DISSING+WEITLING architecture a|s mossmaritime

Concept development, floating bridge E39 Bjørnafjorden

Appendix E – Enclosure 2

10205546-08-NOT-016

Aerodynamic assessment

AAS-JAKOBSEN COWI Multiconsult

JOHS HOLT AkerSolutions entail NGI DISSING+WEITLING architecture a|s mossmaritime

MEMO

PROJECT	**Concept development, floating bridge E39 Bjørnafjorden**	DOCUMENT CODE	10205546-08-NOT-016
CLIENT	Statens vegvesen	ACCESSIBILITY	Restricted
SUBJECT	**AMC status 1 - Aerodynamic assessment**	PROJECT MANAGER	Svein Erik Jakobsen
TO	Statens vegvesen	PREPARED BY	Ketil Aas-Jakobsen
COPY TO		RESPONSIBLE UNIT	AMC

SUMMARY

The aerodynamic assessment is ongoing. Preliminary load coefficients is proposed and more detailed values will be calculated as soon as the cross sections are decided. Aerodynamic stability will be performed on the bridge as a system, and for local components, such as cables in the cable stayed bridge. In-homogeneity in wind is now implemented in wind generator program.

1 Introduction

This document summarizes the planned and performed work for assessment of aerodynamic for the Bjørnafjorden floating bridge.

2 Planned work

The work for assessing aerodynamic on the bridge is grouped into three:

1. Assisting the analysis group to obtain the best aerodynamic data for use in the global analysis. This include calculation of aerodynamic load coefficients.
2. Assess aerodynamic stability of the bridge as a system and individual components, as cables. In addition to buffeting, which are a part of the ordinary analysis, both high wind speed phenomena (gallloping, divergence and flutter) and low speed phenomena (vortex shedding) will be adressed for all relevant components of the bridge.
3. Evaluation of effects of inhomogenity in the wind on structural response.

0	28.01.2019	Status 1 issue	K. Aas-Jakobsen	R. M. Larssen	S. E. Jakobsen
REV.	DATE	DESCRIPTION	PREPARED BY	CHECKED BY	APPROVED BY

3 Status of performed work

3.1 Aerodynamic data

3.1.1 Bridge deck

At the time of writing the cross sections for K11-K14 are not finally decided. When they are confirmed, analysis will be performed in order to obtain drag, lift and moment coefficients, as well as its derivatives. In order to move forward from here results from the wind tunnel tests performed on the cross section from Phase 3 of the project is used /2/.

Figure 1 shows a comparison between the Phase 3 cross section (K7 and K8) and the cross sections that are currently being considered. It is envisioned that fairings will be installed to make the structural cross section more aerodynamic.

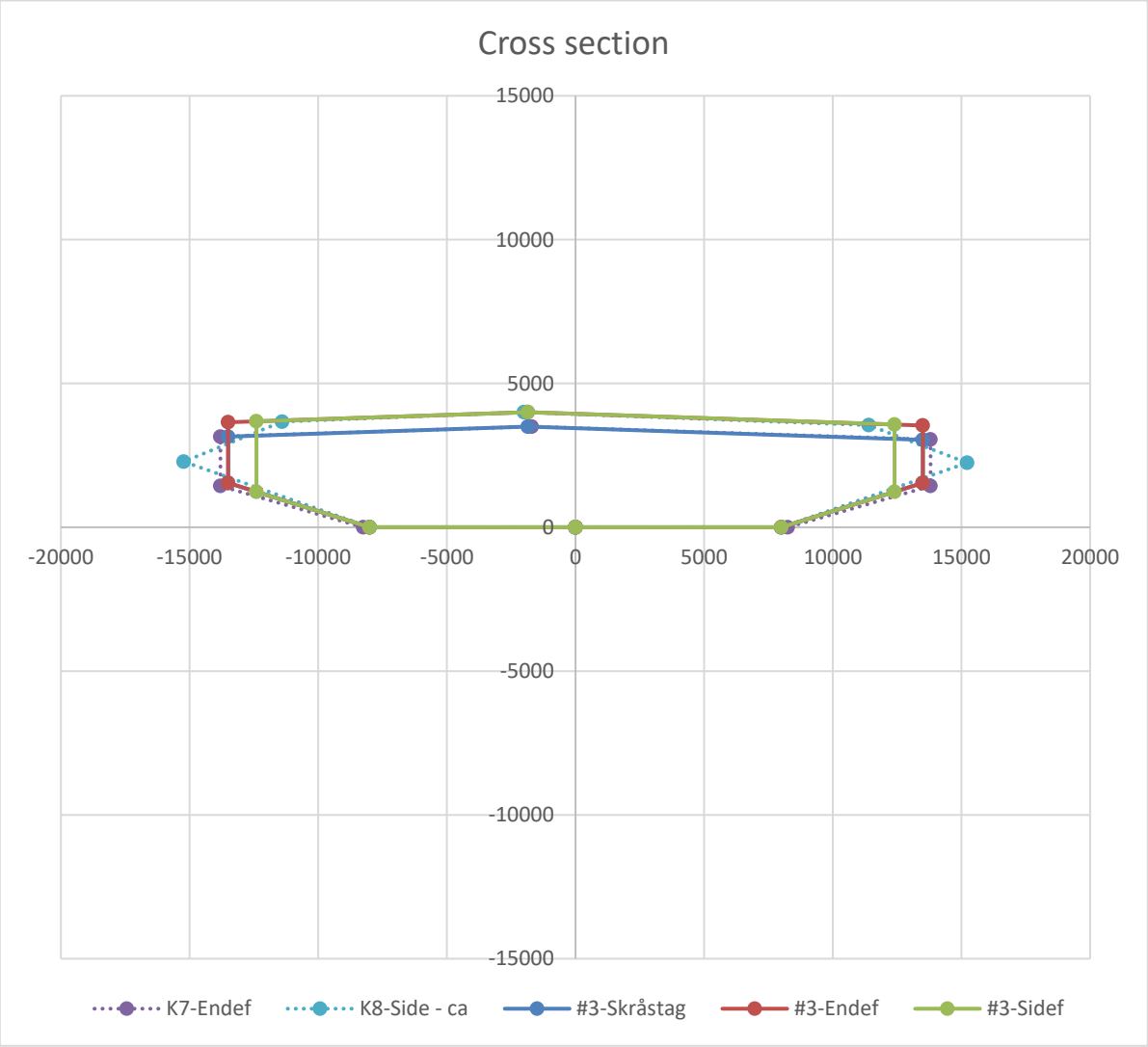

Figure 1 Cross sections from Phase 3 (K7 and K8) compared to current suggested cross section.

Based on the cross section in Phase 3 wind tunnel tests were performed in order to obtain the aerodynamic coefficients. Due to the un-symmetric nature of the cross section, tests were preformed for wind in both directions. Tests were also performed in smooth and turbulent flow. In addition near surface effects was studied by adding a boundary below the bridge deck. Figure 2 shows example of drag coefficient for the K7 option on phase 3.

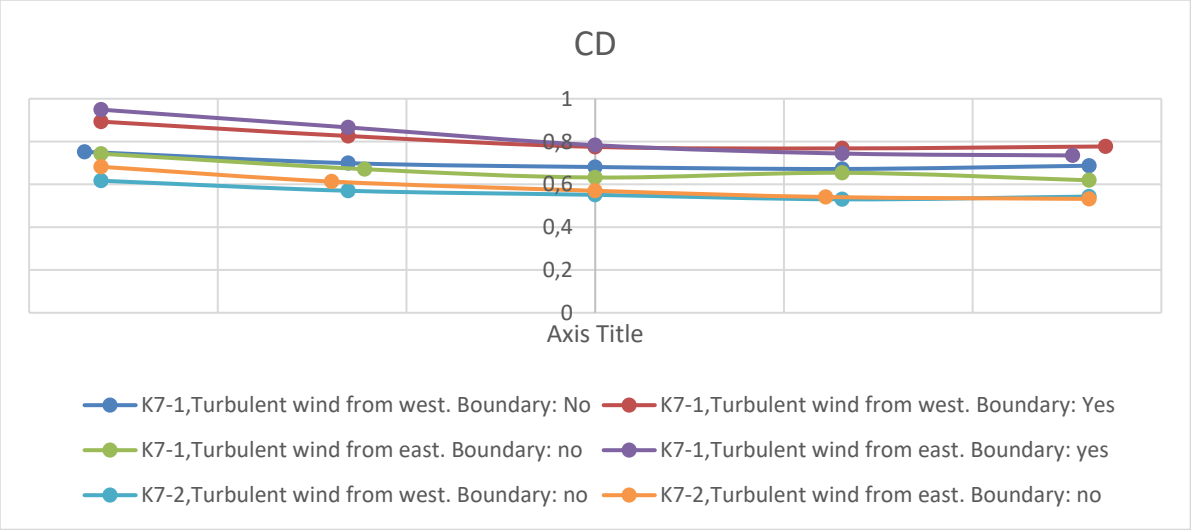

Figure 2 Example of variation of drag coefficient for K7.

Generally, the more conservative values were obtained for wind from one side (east), turbulent flow and when added boundary. Thus, the values in this document were extracted from this case.

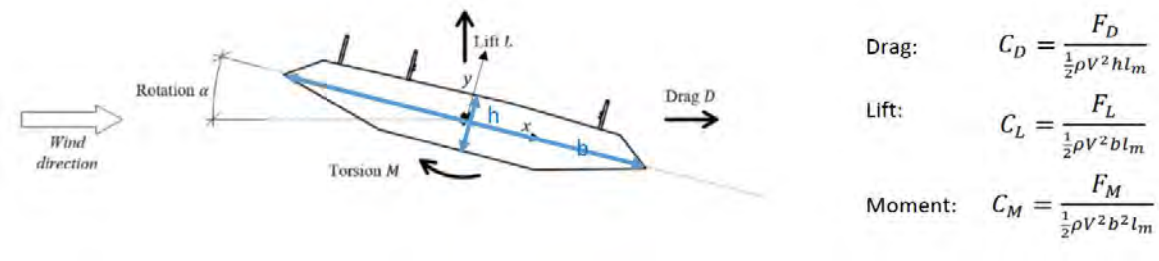

Figure 3 Aerodynamic definitions.

Figure 3 shows definition of the aerodynamic coefficients for the deck. When extracting the these coefficients the following is taken into account:

- A static rotation of the deck of one degree
- A wind direction offset of one degree
- A safety margin to account for other effects (This could e.g. be interaction with the water surface during a storm)

Thus, the most conservative value within +/- 3 degrees is selected. For the derivatives of the main coefficients the value at 0 deg is selected. The wind tunnel tests also show some difference between the K7 and K8 option. The values presented in Table 1 is based on K7 and is considered to be conservative.

Table 1 Suggested aerodynamic load coefficients for preliminary analysis.

	C_D	C_L	C_M	$dC_D/d\alpha$	$dC_L/d\alpha$	$dC_M/d\alpha$
Cross section	0,949	-0,629	-0,076	-2,330	3,591	1,165

3.2 Cables

The drag factor for cables is calculated from /3/ based on a diameter of 200mm. If the diameter of the cables deviates significantly from this a reevaluation is necessary

Table 2 Drag coefficients for cables. Reference length is diamter of cable.

Mean wind speed	**Cd**
Less than 20 m/s	1.2
Above and including 20m/s	0.8

3.3 Square element. Coulmns and pylons.

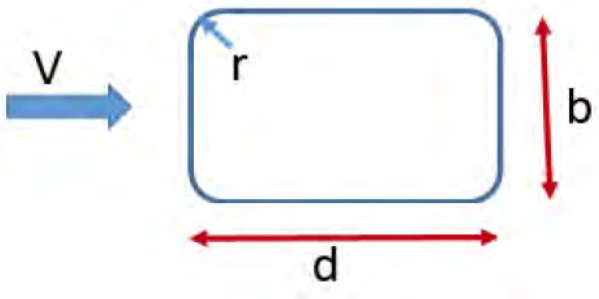

Figure 4 Definitions for drag factor of rectangular cross section.

The suggested values is calculated from /3/ and is based on a corner cut of r=0.7m. For now it is suggested to use a drag value of 1.5 for all aspect ratios. This is conservative for the selected corner cut, see Figure 4 for definitions and Figure 5 for result of calculations.

Shielding effects is not taken into account. Lift and moment coefficients are currently set to zero.

Drag factor columns and pylons: Cd = 1.5

Forces is calculate based on b: e.g. $F=0.5*\rho*Cd*b*V^2$

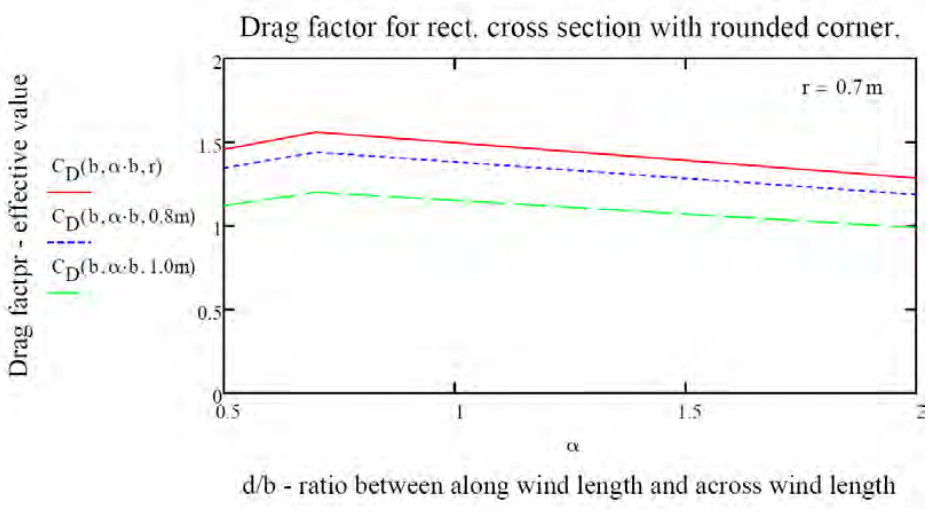

Figure 5 Drag factor for rectangular cross section with rounded corner.

3.4 Pontoons

Wind load on the dry part of the pontoon has not yet been considered.

3.5 Aerodynamic stability

Loss of aerodynamic stability is caused by wind phenomena that interact with the structure, either with the cross sectional shape itself or by interaction with the dynamic property of the structure.

One of the unique feature of the bridge is the length and the associated broad range of vibration periods. Due to the length the first fundamental modes have vibration period ranging from about 120s from the end anchored bridge and 40s for the side anchored, and downwards.

For some of the aerodynamic stability analysis time consuming analysis must be performed. Thus, as an initial approach results from previous phases and best practice is used to address the problem. When the cross sections are decided more detailed properties will be calculated and used in the assessment.

Aerodynamic stability will be addressed when the K11-K14 concepts are more mature. The following is planned:

Bridge as a global system:

- Flutter (Multimode approach)
- Vortex shedding
- Galloping
- Divergence

Cable stayed bridge elements (deck and global behavior is covered by the point above)

- Vortex shedding of cable and tower
- Galloping
- Divergence

3.6 Inhomogenity in wind

Normally, the mean wind speed and turbulence intensity varies only with height. For super-long span bridges there may be different wind properties along the alignment. This could arise from local condition or different meteorological conditions. As a base case the design basis /1/ specifies variation of mean wind speed and turbulence intensity with height, as normal. In addition it specifies varying properties along the alignment. This is in the following referred to as in-homogeneity in wind.

The sensitivity to in-homogeneity in wind is planned to be addressed in the time domain by adjusting the wind time histories that are used as input to the analysis. WindSim, which generated the wind time histories for the time domain analysis, has been updated such that it can handle in-homogeneity in wind. Thus, everything is ready for studying these effects.

4 References

/1/ SBJ-32-C4-SVV-90-BA-001 - Design Basis Bjørnafjorden. Rev 0.

/2/ SBJ-32-C4-SOH-20-RE-001 - Wind model testing for floating bridge, small-scale test, step 1

/3/ NS-EN 1991-1-4:2005+NA:2009. Eurocode 1: Action on structures. Part 1-4: General actions – Wind actions

Concept development, floating bridge E39 Bjørnafjorden

Appendix E – Enclosure 3

10205546-08-NOT-060

Aerodynamic load coefficients sensitivity

AAS-JAKOBSEN COWI Multiconsult

JOHS HOLT AkerSolutions entail NGI DISSING+WEITLING architecture a|s mossmaritime

MEMO

PROJECT	**Concept development, floating bridge E39 Bjørnafjorden**	DOCUMENT CODE	10205546-08-NOT-060
CLIENT	Statens vegvesen	ACCESSIBILITY	Restricted
SUBJECT	**Aerodynamic load coefficient sensitivity**	PROJECT MANAGER	Svein Erik Jakobsen
TO	Statens vegvesen	PREPARED BY	Ketil Aas-Jakobsen
COPY TO		RESPONSIBLE UNIT	AMC

SUMMARY

A parameter study is performed in the time domain to assess the effect of varying aerodynamic load coefficients on the response of bridge concepts K11 and K14 for environmental loading. Fully integrated analysis with wind and wave were run. The main findings are that the sensitivity to change in drag coefficient and slope of the lift coefficient is small for both concepts. An change of the drag factor from 0.8 to 0.9 will increase the peak strong axis moment with about 6% for K11 and 2% for K14. An increase of the slope of the lift coefficient from 3-4 will increase the weak axis moment with about 3% for K11 and 4% for K14 and vertical shear will increase with 8% for K11 and 10% for K14. The response parameters extracted in this analysis shows that K14 generally have lower values than K11.

1 Introduction

This document summarizes the parameter study on the response effect of modifying the aerodynamic load coefficients. The aim of the study is to find guidelines for aerodynamically tuning the cross section to obtain better structural performance of the bridge system.

Figure 1 K11 - Curved floating bridge. Axis 25 indicated

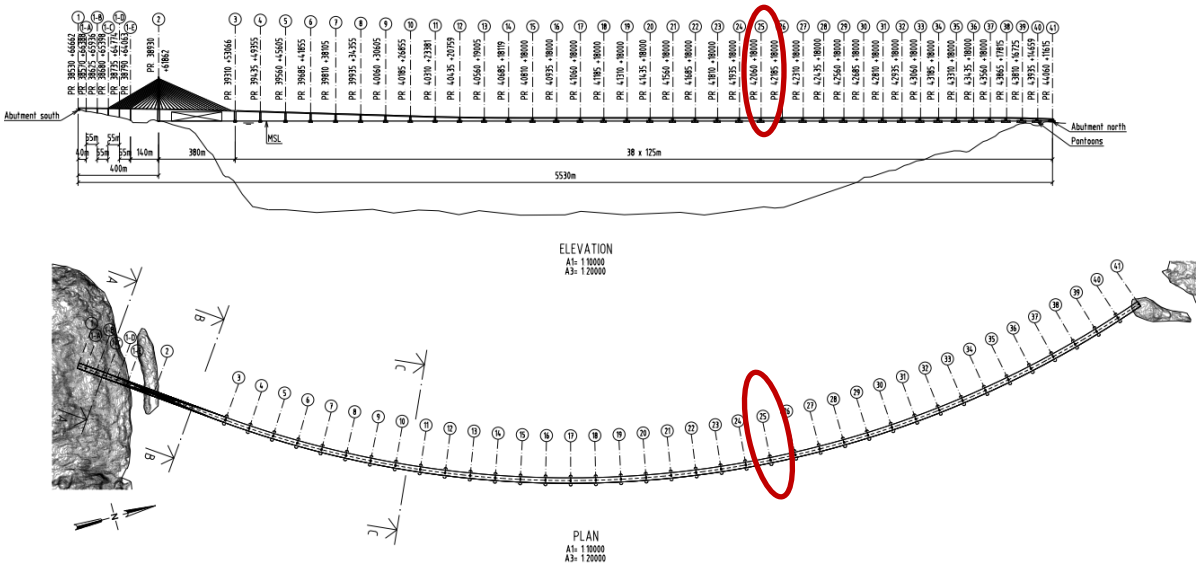

0	29.03.2019	Status 2 issue	K. Aas-Jakobsen	R. M. Larssen	S. E. Jakobsen
REV.	DATE	DESCRIPTION	PREPARED BY	CHECKED BY	APPROVED BY

Figure 2 K14 – S-shaped side anchored floating bridge. Axis 25 indicated.

2 Method

Both K11 (curved floating bridge) and K14 (S-shaped side anchored floating bridge), was used for these analysis. Key response parameters were tracked in order to study the sensitivity to change of the aerodynamic load coefficients.

Currently the deck cross section is made out of purely functional and static considerations and the nose shape is not decided yet, see Figure 3.

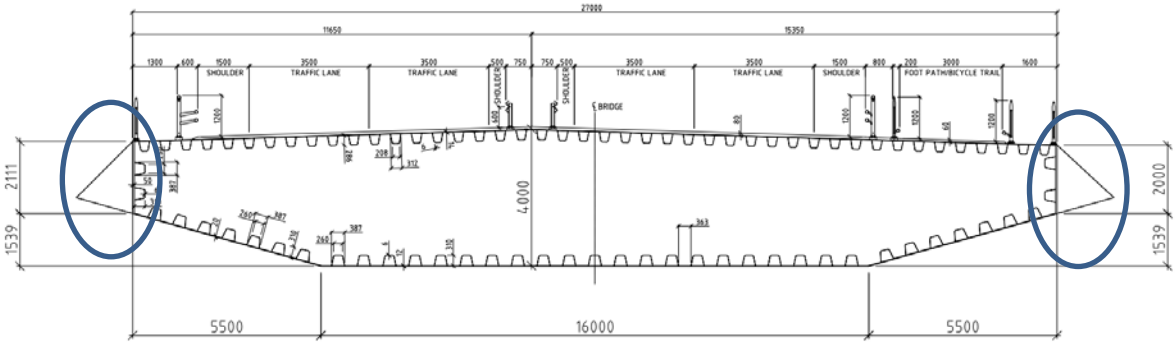

Figure 3 Typical cross section. Nose shape not can be changed.

Figure 4 shows the definition of the aerodynamic load coefficients. Based on wind tunnel tests /2/ reference values were chosen, see Table 1.

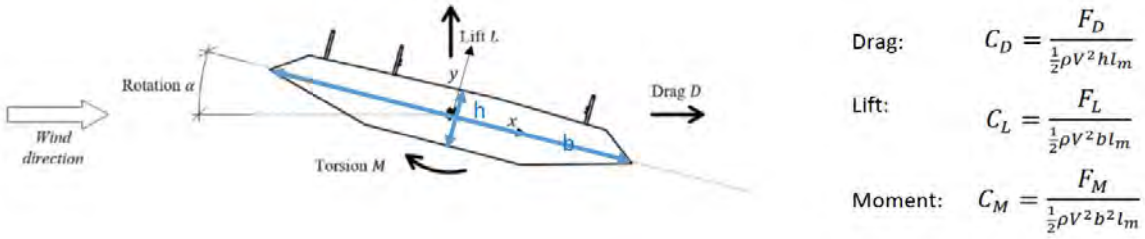

Figure 4 Aerodynamic definitions.

Table 1 Reference aerodynamic load coefficients for sensitivity analysis.

	C_D	C_L	C_M	$dC_D/d\alpha$	$dC_L/d\alpha$	$dC_M/d\alpha$
Cross section	0,80	-0,45	-0,01	-2,30	3,5	1,15

Previous phases has seen that wave action is reduced due to aerodynamic damping. In the drag direction aerodynamic damping is dependent on Cd, while in the vertical direction it is dependent on dCl. These factors, particularly the Cd, will also result in increased forces. However, it is not clear if changing these values will result in reduced overall design forces or not. Thus, the sensitivity was performed based on the reference aerodynamic load coefficients where the following was varied (keeping the other values constant):

- Cd; varying from 0.4 to 1.3
- dCl; varying from 1.0 to 5.0

The analysis was performed with wind and wave perpendicular to the bridge for ULS cases.

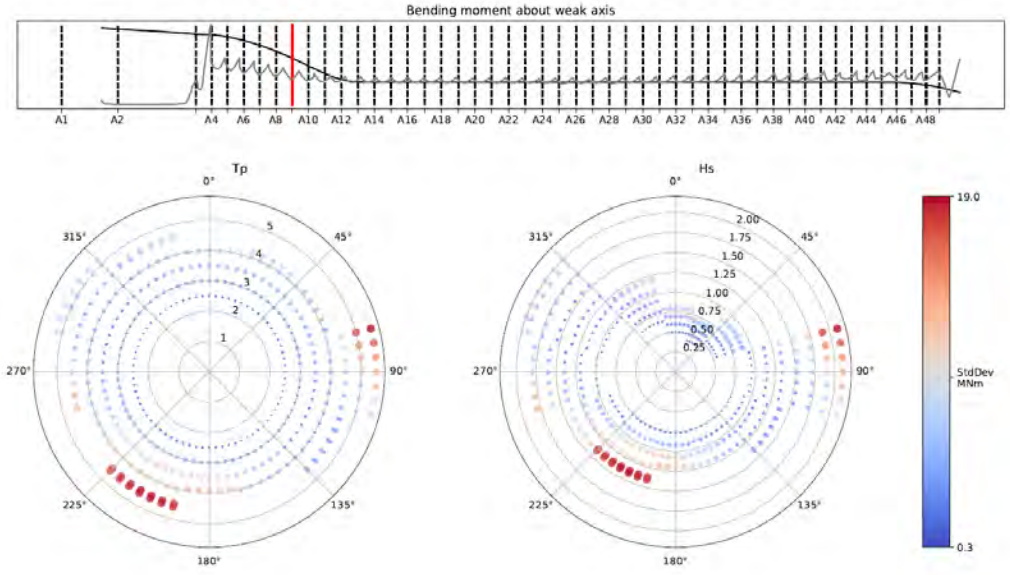

Figure 5 Model and results from screening analysis. This sensitivity analysis was performed for wind from 90 deg.

3 Results

Results were extracted for all elements in the bridge. A more detailed study of the results were performed at axis 25, which is fairly representative for the low part of the bridge, see Figure 1.The following results were extracted: Displacement (x,y,z and rotation), associated accelerations, week axis moment, strong axis moment and torsional moment. Based on a screening of the results the week and strong axis moment and the vertical acceleration shows most sensitivity for the varied parameters.

Results are presented as mean values, standard deviation and peak value estimated as mean plus three times the standard deviation. Based on a screening of the results the strong axis moment, week axis moment and vertical acceleration is reported.

3.1 Results for whole bridge

Figure 6 - Figure 9 shows the results for peak of the strong axis and week axis along the bridge axis for both concepts. Results for other components is available upon request.

K11 – curved bridge

The strong axis moment has its highest values at the tower and at the north abutment. It is also worth noting that the values are higher in the transition part of the bridge, where the bridge deck ramp down from the high bridge to the low bridge part, than in the lower part.

The week axis moment has peak values at each pontoon and mid point between pontoons. There is also a pronounced peak near the transition from the high bridge to the floating bridge. Due to the horizontally curved shape of K11, some pontoons will have inclinations towards the incoming waves. This results in increased weak axis moment in part of the bridge. For this analysis these values are found towards the north abutment.

K14 – S-shaped side anchored bridge.

For K14 the strong axis moment is governed by the anchor connection points. The strong axis moment is higher in the floating part than in the high bridge and the highest strong axis moment is found near the north abutment.

The week axis moment has high values towards south and north. The peak value is found in the transition between the high bridge and floating part. The week axis moment is also large in the transition area where the bridge deck ramps down from the high bridge to the low bridge part. At the middle of the bridge the weak axis moment is smaller, but it ramps up when approaching the north abutment.

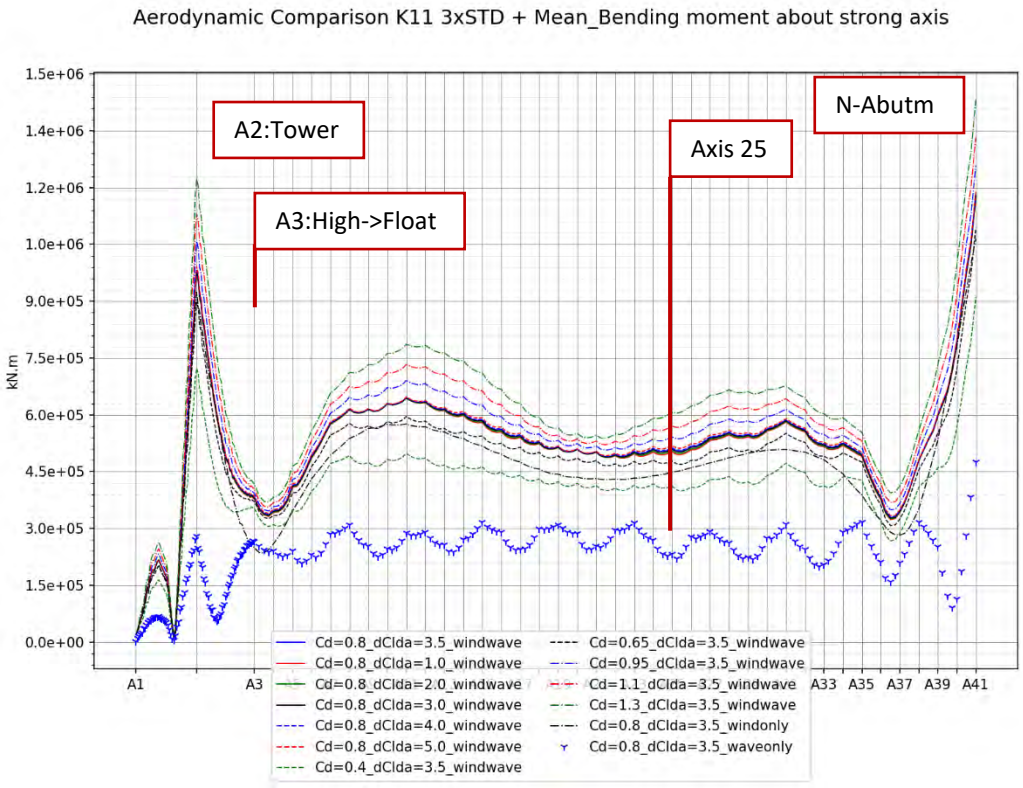

Figure 6 K11 - Peak bending about strong axis.

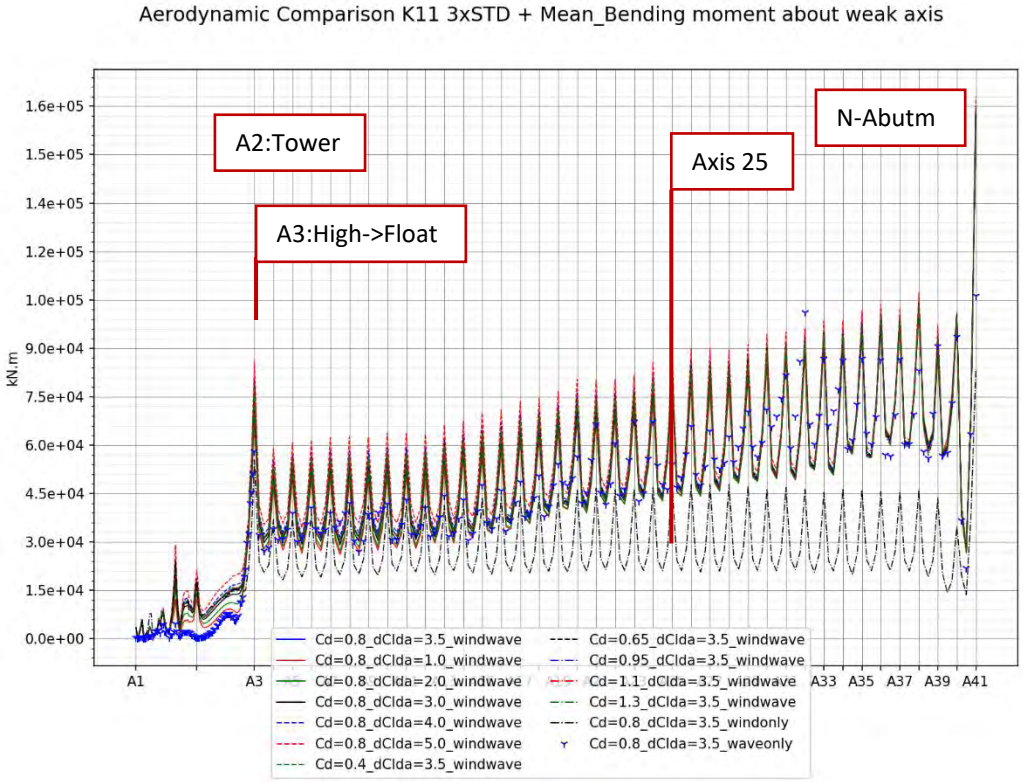

Figure 7 K11 - Peak bending moment about week axis.

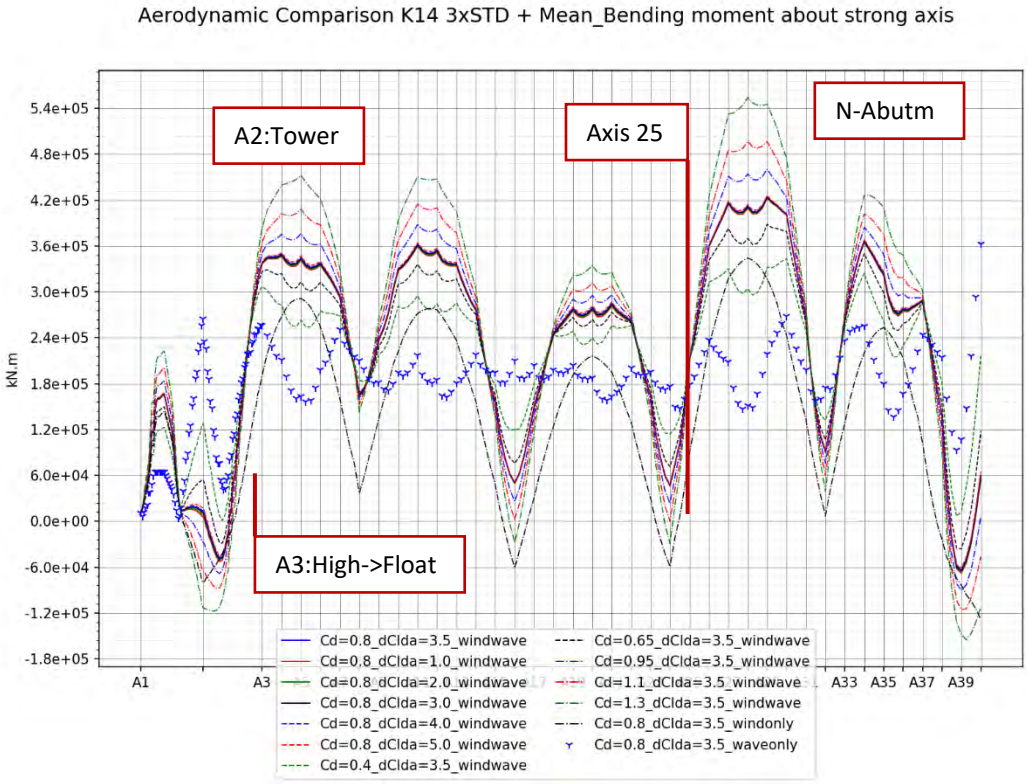

Figure 8 K14 - Peak bending moment about strong axis.

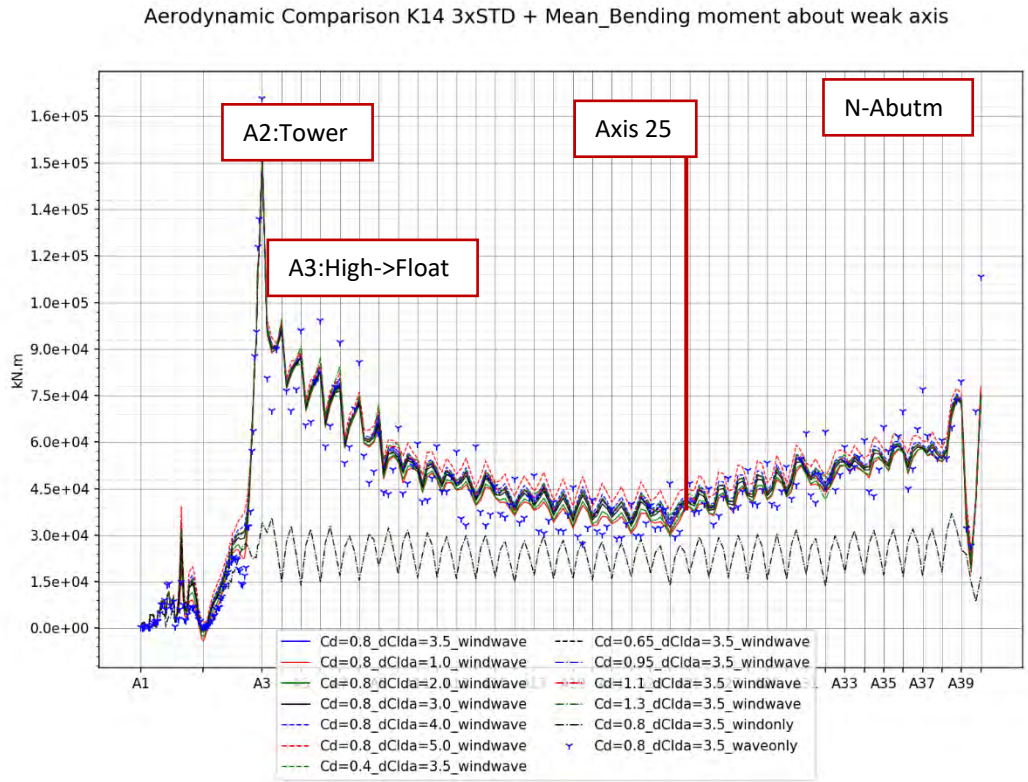

Figure 9 K14 - Peak bending moment about week axis.

3.2 Axis 25 results – Mean Value

Selected mean values in Axis 25 is shown in Figure 10. The general trend is that the strong axis moment increase with Cd and the week axis moment increase with dCl for both concepts.

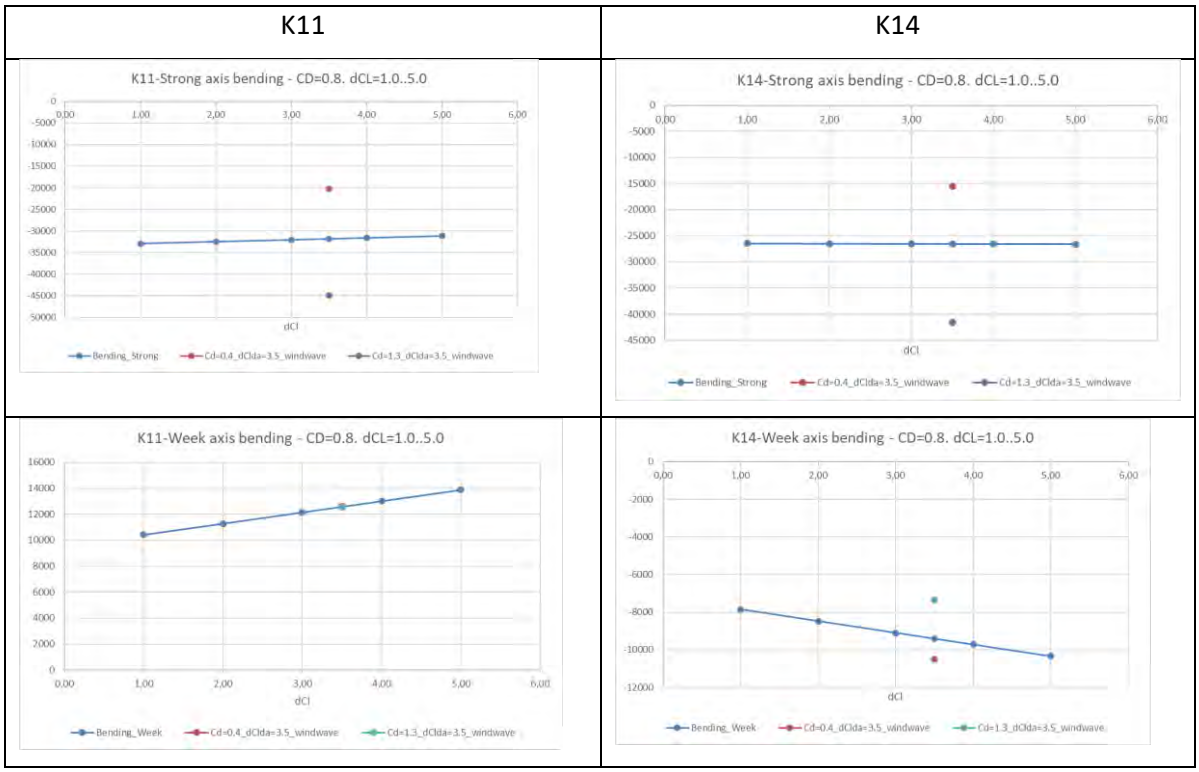

Figure 10 Mean values. Key results. Left: K11. Right: K14. Row 1: Strong axis bending [kNm]. Row 2: Week axis bending [kNm].

3.3 Axis 25 results – Standard Deviation

Plots of the standard deviation is shown in Figure 11.

Strong axis moment.
For K11 the strong axis moment increases with the Cd, but is unaffected by change of dCl.
For K14 the it increases with Cd and increases slightly with with dCl.

Week axis moment
For both K11 and K14 the week axis moment increases with dCl and is almost independent on Cd.

Transverse acceleration.
There are only minor changes of transverse acceleration with change of Cd and dCl for both concepts.

Vertical acceleration.
There are only small changes of transverse acceleration with change of Cd and dCl for both concepts.

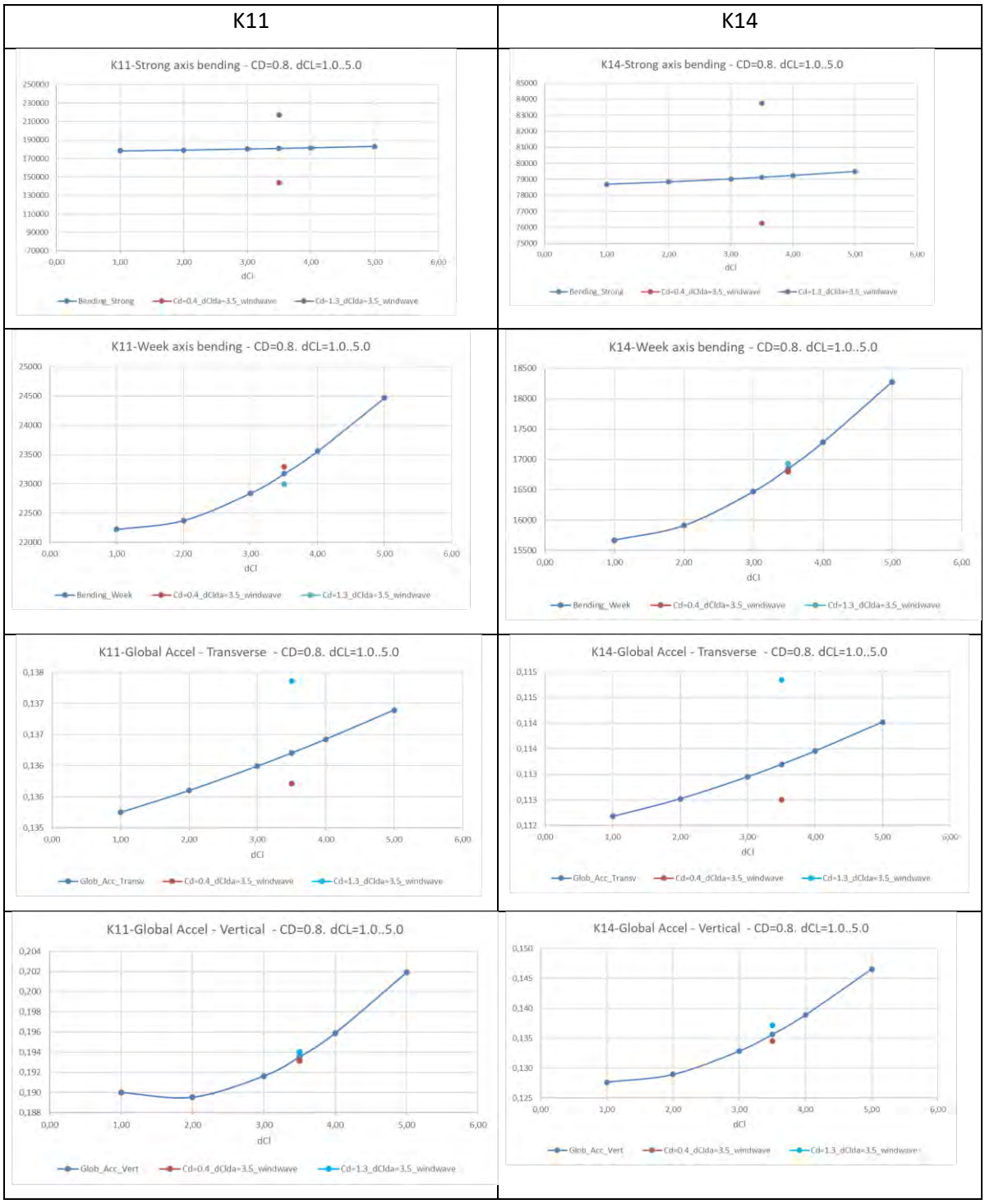

Figure 11 Standard deviation. Key results. Left: K11. Right: K14. Row 1: Strong axis bending [kNm]. Row 2: Week axis bending [kNm]. Row 3: Transvers acceleration [m/s^2] Row 4: Vertical acceleration [m/s^2].

3.4 Axis 25 results – Peak Values

The peak values in axis 25 is shown in Figure 12.

Strong axis moment.
For both K11 and K14 the strong axis moment increases with the Cd, but is independent on dCl.
Week axis moment
For both K11 and K14 the week axis moment increases with dCl and is almost independent on Cd.
Transverse acceleration.
There are only minor changes with change of Cd and dCl for both concepts.

Vertical acceleration.

There are only small changes with change of Cd and dCl for both concepts.

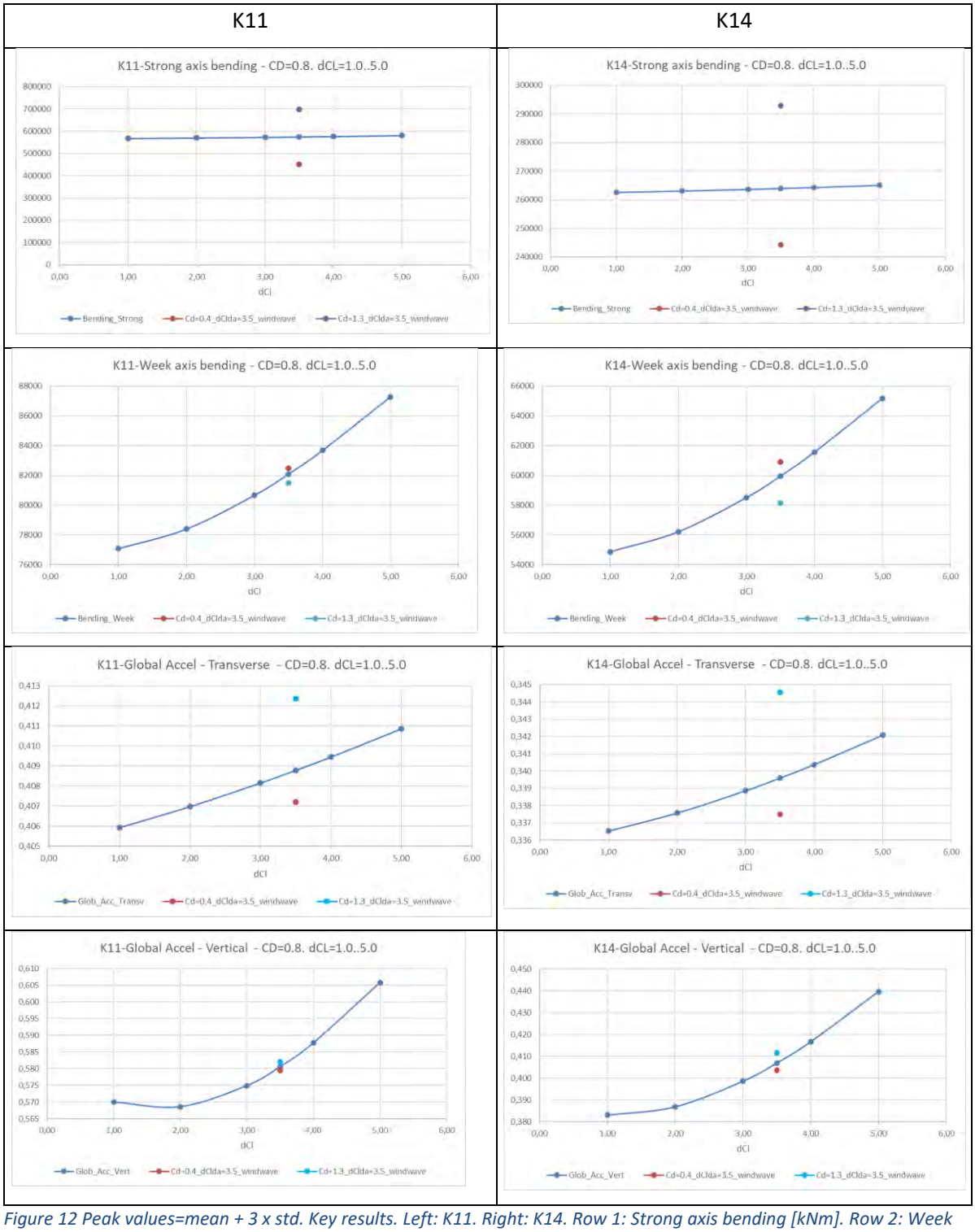

Figure 12 Peak values=mean + 3 x std. Key results. Left: K11. Right: K14. Row 1: Strong axis bending [kNm]. Row 2: Week axis bending [kNm]. Row 3: Transvers acceleration [m/s^2] Row 4: Vertical acceleration [m/s^2].

4 Discussion and conclusion

Table 2 give a numeric summary of typical values of forces, displacement and accelerations and their sensitivity to change of aerodynamic parameters for the analyzed case. A general observation from the selected results in Table 2 is that the values for K14 are lower than K11.

*Table 2 Sensitivity for change of aerodynamic parameters. ULS value calculated as Peak = Mean + 3.0 * std. Axis 25.*

SUMMARY	**K11**			**K14**		
	Cd=0.8 dCl=3.5	**Cd 0.4->1.3**	**dCl 1.0->5.0**	**Cd=0.8 dCl=3.5**	**Cd 0.4->1.3**	**dCl 1.0->5.0**
Change input:		225 %	400 %		225 %	400 %
Strong axis mom.:	575MNm	54 %	2 %	264MNm	20 %	1 %
Weak axis mom.:	82MNm	-1 %	13 %	60MNm	-5 %	19 %
Vertical shear:	1.8MNm	0 %	35 %	1.4MNm	-7 %	50 %
Transverse displ.:	8.0m	85 %	2 %	5.9m	148 %	1 %
Transverse acc.:	0.41m/s^2	1 %	1 %	0.34m/s^2	2 %	2 %
Vertical displ:	0.49m	0 %	8 %	0.62m	-5 %	23 %
Vertical acc:	0.58m/s^2	0 %	6 %	0.41m/s^2	2 %	15 %

The change of aerodynamic parameters have the following effect on the results in axis 25:

A change of Cd with a value of 0.1 (i.e. Cd from 0.8->0.9):

- Strong axis moment is increased with about 6% for K11 and 2% for K14.
- Transverse displacement will increase with 10% for K11 and 16% for K14.
- For the other response values the changes are small.

A change of dCl from 3.0->4.0 will have the following effects:

- Weak axis momen increase with 3% for K11 and 4% for K14.
- Vertical shear increase with 8% for K11 and 10% for K14.

This analysis indicate that the current design is not particularly sensitive to the choice of aerodynamic parameters.

5 References

/1/ SBJ-32-C4-SVV-90-BA-001 - Design Basis Bjørnafjorden. Rev 0.

/2/ SBJ-32-C4-SOH-20-RE-001 - Wind model testing for floating bridge, small-scale test, step 1

/3/ NS-EN 1991-1-4:2005+NA:2009. Eurocode 1: Action on structures. Part 1-4: General actions – Wind actions

Concept development, floating bridge E39 Bjørnafjorden

Appendix E – Enclosure 4

10205546-08-NOT-061

Wind load coefficients – Storebælt

MEMO

PROJECT	**Concept development, floating bridge E39 Bjørnafjorden**	DOCUMENT CODE	10205546-08-NOT-061
CLIENT	Statens vegvesen	ACCESSIBILITY	Restricted
SUBJECT	**Wind Load Coefficients - Storebælt**	PROJECT MANAGER	Svein Erik Jakobsen
TO	Statens vegvesen	PREPARED BY	Allan Larsen
COPY TO		RESPONSIBLE UNIT	AMC

SUMMARY

This memo summarizes aerodynamic load coefficients measured for variants of the Storebælt East Bridge deck cross sections

0	29.03.2019	Status 2 issue	A. Larsen	K. Aas-Jakobsen	S. E. Jakobsen
REV.	DATE	DESCRIPTION	PREPARED BY	CHECKED BY	APPROVED BY

1 Introduction

This memo summarises wind load coefficients measured for variants of the deck sections of the Storebælt East Bridge (main suspended spans and approaches) during tender evaluation, /1/, /2/.

2 Storebælt East Bridge

The storebælt East bridge is composed of two multi-span steel beam bridges (approaches) leading up to a three span suspension bridge.

2.1 Approach Bridges

The approach bridges have individual span lengths of 193 m between piers. This dictates a section depth of 6.7 m. The geometry of the trapezoidal box cross section referred to as A1.1 is shown in Figure 2.1

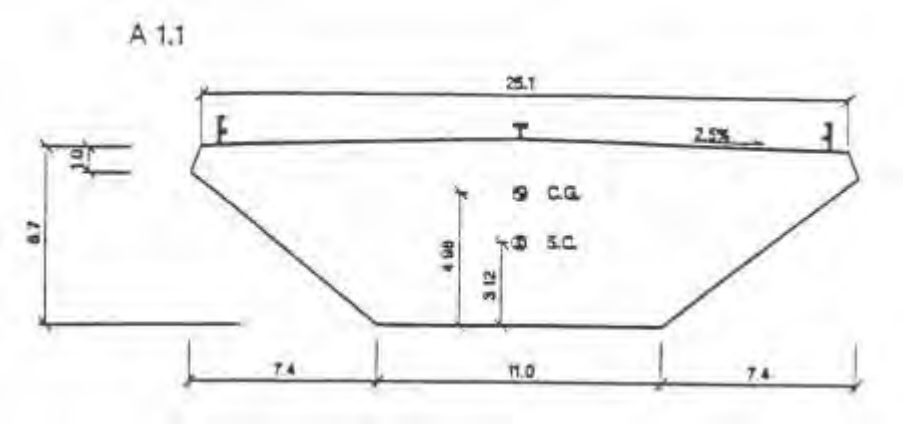

Figure 2.1 A1.1 deck cross section, Approaches, Storebælt East Bridge.

The end spans closest to land are relatively close to the sea surface in terms of the section depth (approximately 10 m). The effect of the proximity of the sea surface on the aerodynamic load coefficients was investigated separately in a wind tunnel test where the deck section was set close to the wind tunnel floor (ground plane), section A1.3, Figure 2.2.

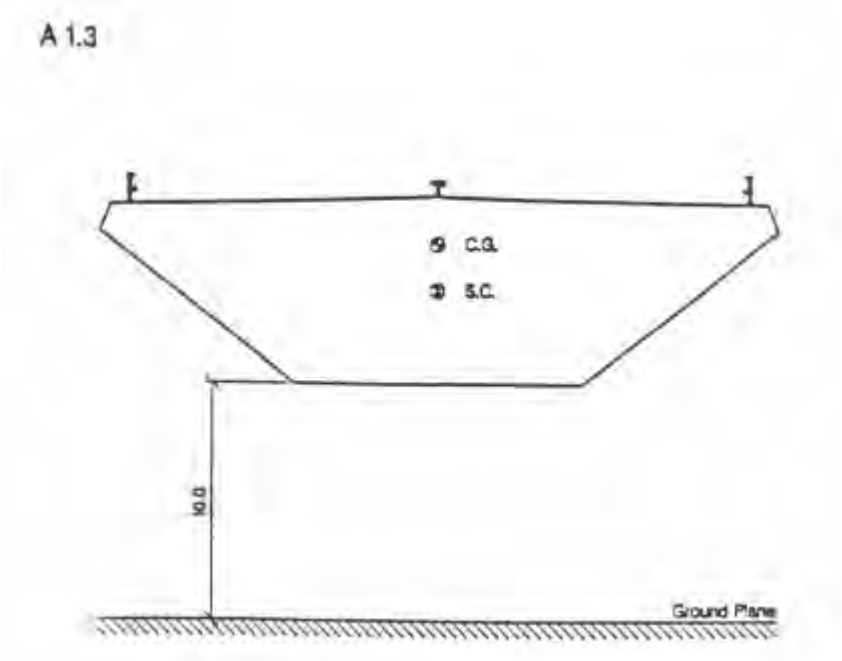

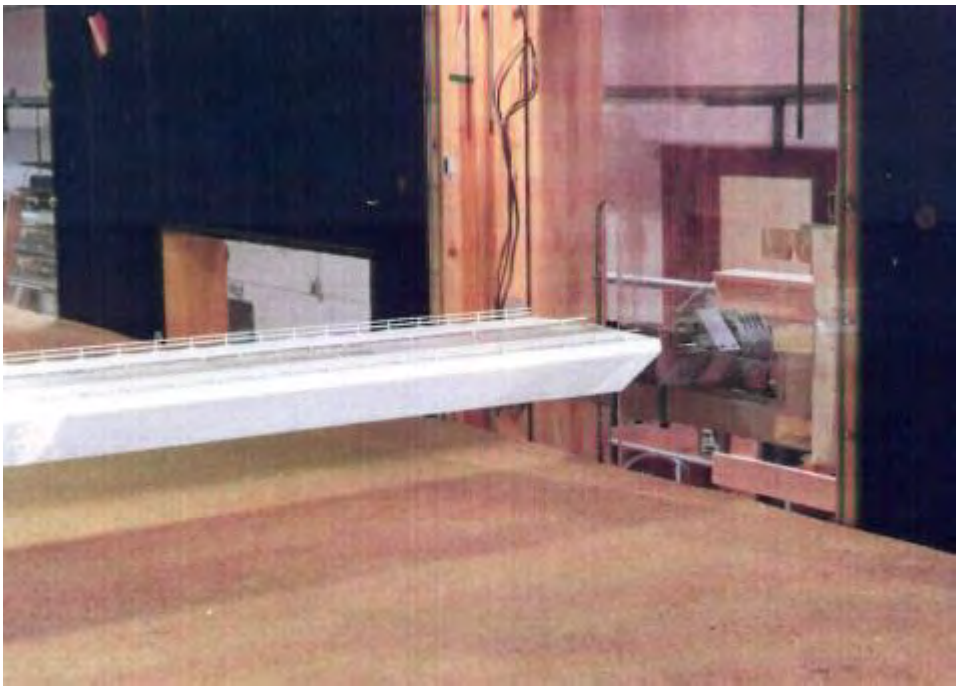

Figure 2.2 A1.3 Deck section (A1.1 set 10 m above wind tunnel ground plane), Approaches, Storebælt East bridge.

2.2 Suspension Bridge

The trapezoidal deck section of suspension bridge referred to as H9.1 is 4 m deep and 31 m wide, Figure 2.3.

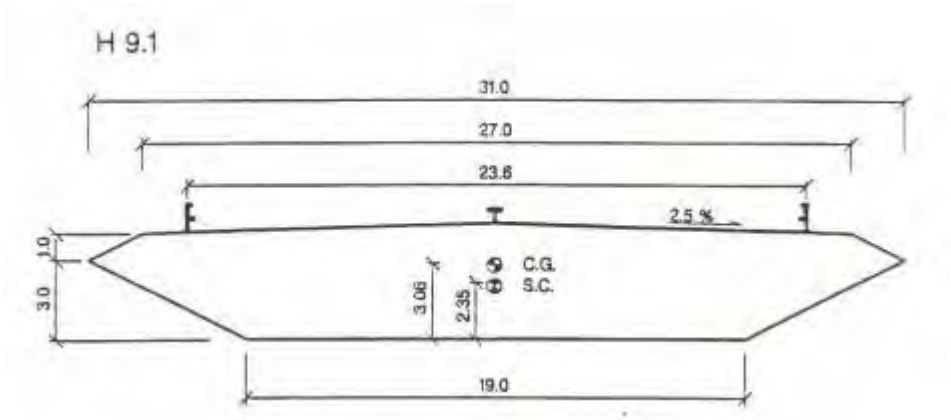

Figure 2.3 H9.1 deck section, suspension bridge, Storebælt East Bridge.

During tender evaluation it was desirable to investigate other cross section geometries with a view to save material without deteriorating aerodynamic properties. Three alternative cross sections H9.4, H10.1 and H11.1 were tested with the objective of clarifying the influence of geometry on the wind load coefficients.

The H9.4 cross section has the same 4 m depth as the H9.1 cross section but the triangular noses were truncated to produce a 28 m wide deck, Figure 2.4.

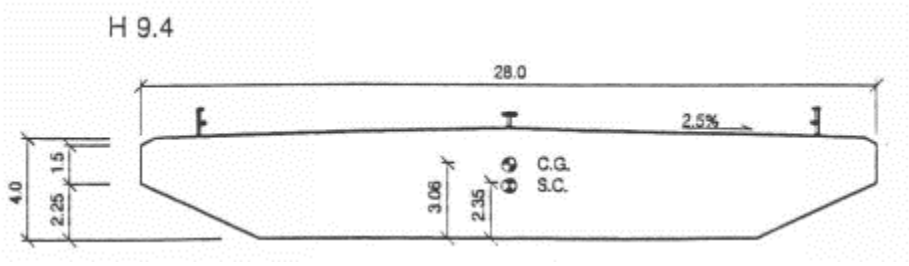

Figure 2.4 Alternative H9.4 deck section, suspension bridge, Storebælt East Bridge.

The H10.1 cross section has a decreased depth of 3 m but retained the over-all trapezoidal geometry and deck width of 31 m, Figure 2.5.

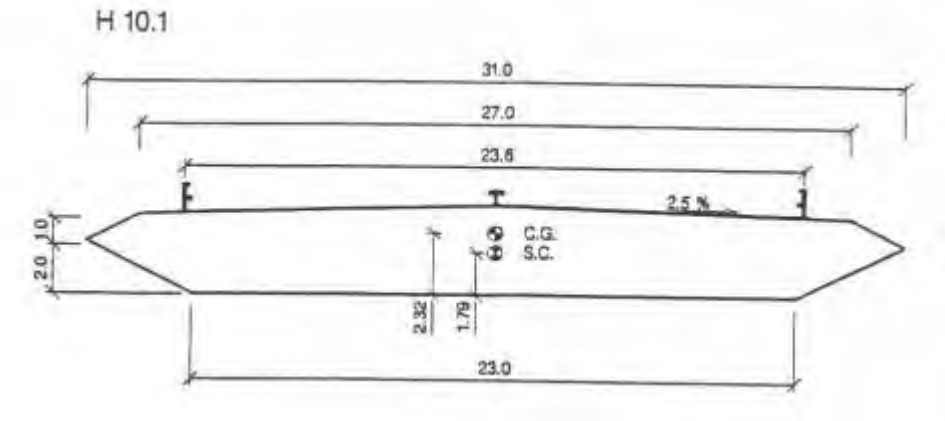

Figure 2.5 Alternative H10.1 deck section, suspension bridge, Storebælt East Bridge.

A final variation of the suspension bridge deck section H11.1 retained the 3 m section depth and 31 m deck width but featured curved lower side panels in an attempt to reduce the aerodynamic drag force, Figure 2.6.

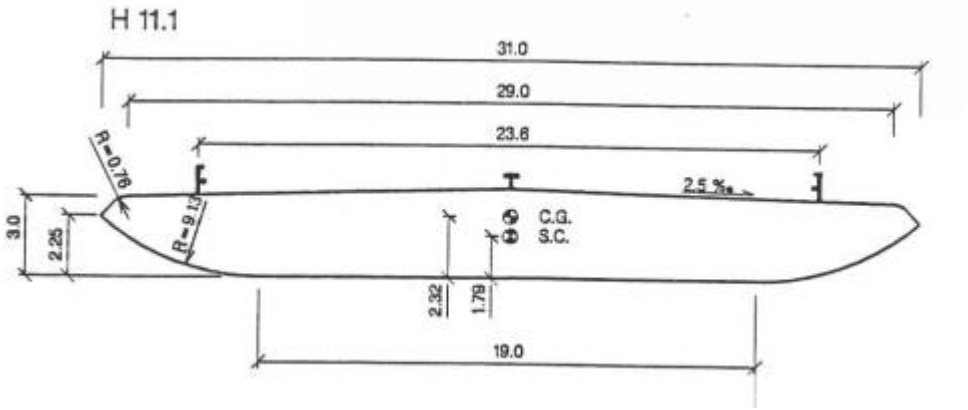

Figure 2.6 Alternative H11.1 deck section, suspension bridge, Storebælt East Bridge.

3 Wind load coefficients

The wind load coefficients for the above mentioned deck cross sections are reported in tabular form below. Drag C_D, Lift C_L and moment C_M coefficients are obtained making the measured sectional Lift, Drag and Moments non-dimensional by the dynamic head $\frac{1}{2}\rho V^2$ and the over all section width B = 31 m for the suspension bridge sections and B = 25.8 m for the approach bridge sections. The moment is made non-dimensional by B^2.

$$C_{D,L} = \frac{D,L}{½\rho V^2 B}$$

$$C_M = \frac{M}{½\rho V^2 B^2}$$

The wind tunnel measurements demonstrated that the wind load coefficients obeyed a linear relationship with the angle of attack α in an range of -5 deg < α < +5 deg as demonstrated for the lift in Figure 3.1.

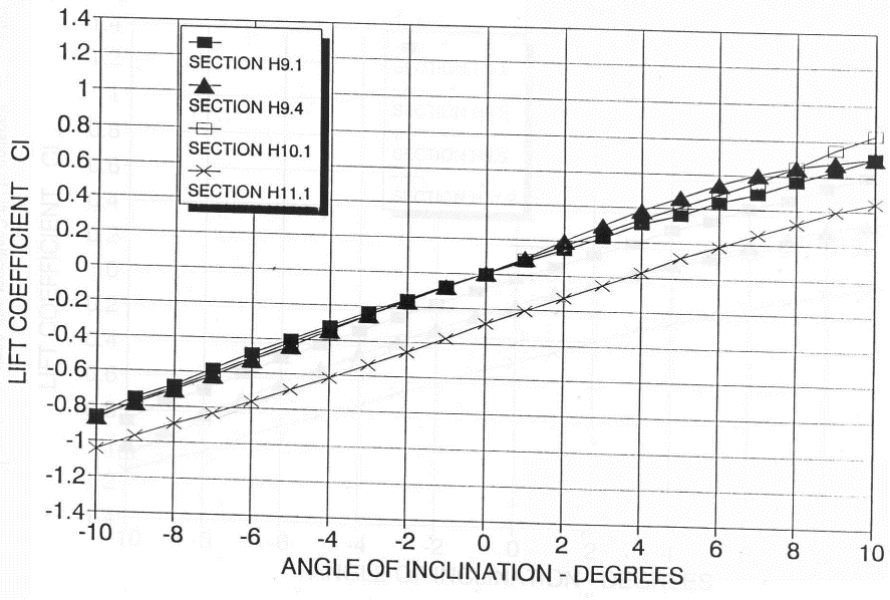

Figure 3.1 Measured lift coefficient as a function of angle of attack for the suspension bridge cross sections.

In view of the linear relationship demonstrated in Figure 3.1 the wind load coefficients for all deck cross sections are presented as coefficients $C_{D0,L0,M0}$, $dC_{D,L,M}/d\alpha$ fitting the linear relationship,

Table 3.1:

$$C_{D,L,M}(\alpha) = C_{D0,L0,M0} + \left(dC_{D,L,M}/d\alpha\right) \cdot \alpha$$

Table 3.1 Wind load coefficients for cross sections A1.1, A1,3, H9.1, H9.4, H10.1, H11.1

Section	C_{D0}	$dC_D/d\alpha$ rad^{-1}	C_{L0}	$dC_L/d\alpha$ rad^{-1}	C_{M0}	$dC_M/d\alpha$ rad^{-1}
A1.1	0.186	0	0.006	4.58	0.118	0.52
A1.3	0.192	0	0.213	5.87	0.142	0.89
H9.1	0.077	0	0.01	4.8	0.02	1.16
H9.4	0.078	0	0.01	4.5	0.02	1.18
H10.1	0.081	0	0.01	4.6	0.00	1.14
H11.1	0.070	0	-0.29	4.7	-0.01	1.16

From Table 3.1 the following observations are made:

Approach bridge cross section:

- The proximity of the sea surface (ground plane) has little effect on the drag loading but increases the uplift substantially. En effect that may be important for the ballasting of the end spans.
- The proximity of the sea surface also increases the lift and moment slopes indicating that the end spans recives larger gust wind loading than the more elevated spans.

Suspension bridge cross sections:

- Changes made to the cross section geometry only has an insignificant effect on the drag loarding for the cross sections composed of flate plate panels. This includes truncation of the triangular noses.
- Curving of the side panels (section H11.1) leads to a 5% reduction of the drag loading but introduces a substantial downward lift at 0 angle of attack as compared to the straight panel sections.

4 References

/1/ Tender Evaluation, Approach Bridges, Section Model Tests 1. DMI Document No. 91047-10.00. Restricted.

/2/ Tender Evaluation, Suspension Bridge Alternative Sections, Section Model Tests 1. DMI Document No. 91023-10.00. Restricted.

Concept development, floating bridge E39 Bjørnafjorden

Appendix E – Enclosure 5

10205546-08-NOT-062

CFD analysis of cross sections

AAS-JAKOBSEN COWI Multiconsult
JOHS HOLT AkerSolutions entail NGI DISSING+WEITLING architecture a|s mossmaritime

MEMO

PROJECT	Concept development, floating bridge E39 Bjørnafjorden	DOCUMENT CODE	10205546-08-NOT-062
CLIENT	Statens vegvesen	ACCESSIBILITY	Restricted
SUBJECT	CFD analysis of cross section	PROJECT MANAGER	Svein Erik Jakobsen
TO	Ketil Aas Jakobsen	PREPARED BY	Mitja Papinutti
COPY TO	Statens vegvesen	RESPONSIBLE UNIT	AMC

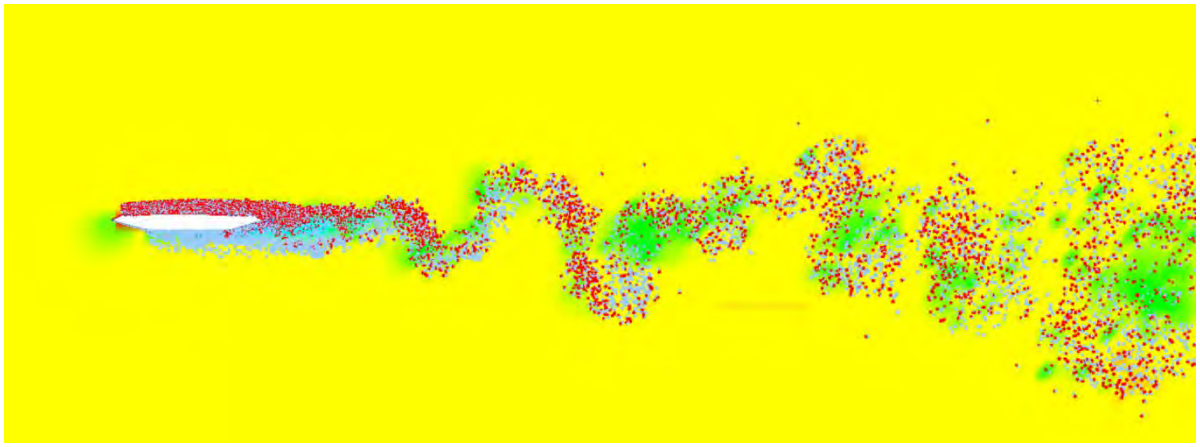

SUMMARY

This memo contains a numerical evaluation of cross-sectional aerodynamics. The vortex particle CFD tool inside commercial software package RM Bridge was used in these investigations. The CFD tool is commonly used for bridge aerodynamics design used for steady aerodynamics, unsteady aerodynamics, vortex shedding vibrations. This memo focuses on evaluating the Quays-Steady State (QSS) coefficients for the selected cross section. First CFD model is calibrated and compared to the wind tunnel tests from 3rd phase of BJF project. Optimal parameters were found and results were compared. The method was then applied on the investigation of the applicability of different cross-section wind shields at the nose of the deck section. Several variations of wind shield noses, a blunt nose, triangular, rounded nose were analyzed. Their aerodynamic performance was applied in a search for the most suitable candidate for side and end anchored floating bridge concepts. In order to ensure aerodynamically stable cross section, galloping and torsional divergence were investigated. All cross section are showing sufficient performance, except for the round nose showing a possible galloping instability. Thus, the round nose is not recommended. The effect of guide vanes was also studied on aerodynamic and aeroelastic performance. In general, flow-controlled measurements confirmed a reduction of the inclination of the lift coefficient. Associated flutter coefficients indicate that the guide vanes increase the aerodynamic damping, as well lower the vortex shedding vibrations. This shows further aerodynamic improvement possibilities.

01	24.05.2019	Final issue	M. Papinutti	K. Aas-Jakobsen	S. E. Jakobsen
00	29.03.2019	Status 2 issue	M. Papinutti	K. Aas-Jakobsen	S. E. Jakobsen
REV.	DATE	DESCRIPTION	PREPARED BY	CHECKED BY	APPROVED BY

1 CFD analysis

Theory background

In RM Bridge, a CFD module is available for computing the aerodynamic coefficients C_D, C_L, C_M of different cross-sections. The plane airflow around an obstacle is generally described by the two-dimensional Navier-Stokes equation for incompressible fluids with constant viscosity and by the resulting vorticity transport equation:

$$\frac{\partial \omega}{\partial} + (\boldsymbol{u} \cdot \nabla)\omega = v\Delta\omega$$

Where

u = is the velocity of the fluid
ω = is the curl of this velocity (vorticity)
v = is the kinematical viscosity of air (0.000015 m^2/s at 20°C)

This equation is numerically solved with consideration of the appropriate boundary conditions.
The method used is the Discrete Vortex Method (DVM). The key points of this method are:

- Representing the outline of the cross section by a number *NrPanels* of straight lines (panels)
- Representing the vorticity field ω by an ensemble of discrete vortex particles of given circulation and core size.

The advantage of this approach is that it is a grid-free method. Consequently, it does not impose further problems to consider also moving cross sections. The principal steps of the operator splitting solution procedure are as follows:

1. Initializing the geometry according to the given cross section.
2. Entering a time stepping loop with time step *dt* for *MaxIterations* iterations.
3. Enforcing the boundary conditions (conservation of total circulation, fixed oncoming flow with velocity and direction angle) and computing aerodynamic loads.
4. Convection of the free vortex particles (second term of left-hand side in the equation above).
5. Diffusion of the free vortex particles (right-hand side in the equation above).
6. Creating new vortex particles at the cross-section surface.
7. Performing housekeeping (delete particles which entered the body, move body, etc.).
8. Proceeding to next time step if necessary.

For further reading you might refer to:

1. Spalart, P.R, Vortex Methods for Separated Flows, NASA TM 100068, NASA, 1988.
   Walther, J.H., Discrete Vortex Method for Two-Dimensional Flow past Bodies of Arbitrary Shape Undergoing Prescribed Rotary and Translational Motion, PhD Thesis, Technical University of Denmark, Lyngby, 1994.
2. Morgenthal, G., Aerodynamic Analysis of Structures Using High-resolution Vortex Particle Methods, PhD Thesis.
3. RM user manual, Bentley 2008, Graz.

Calibration

The vortex particle method was calibrated on the cross section "K7-EndAnchored". The wind tunnel tests from previous 3rd phase of BJF project were providing as reference values. The goal is to extract similar CFD values compared to wind tunnel tests. Several parameters were calibrated in order to achieve reasonable accuracy and performance. Validation section is depicted in Figure below:

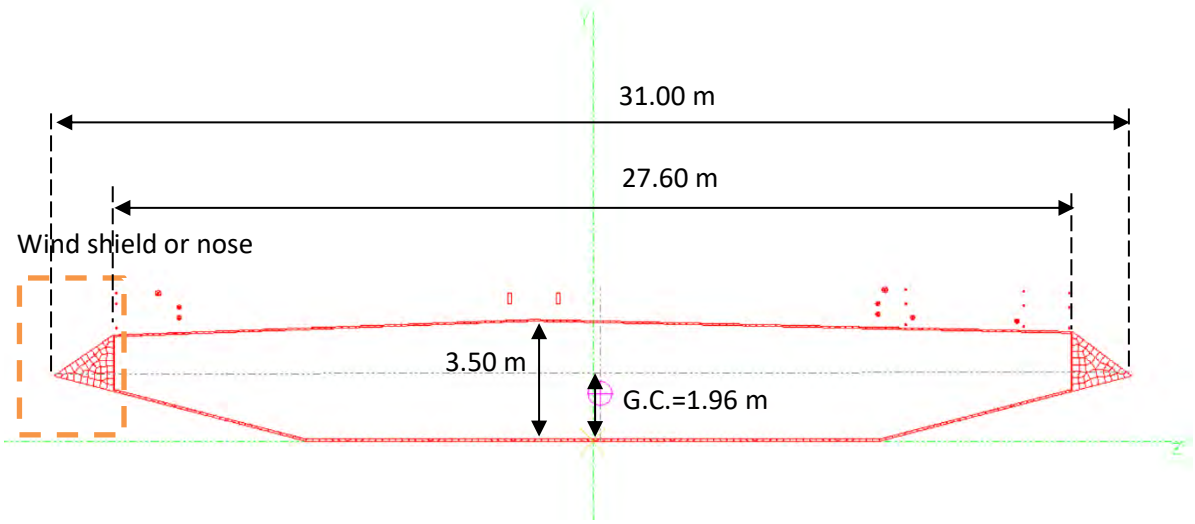

Figure: K7-EndAnchored cross section with railings.

All aerodynamic forces are submitted to a gravity center of cross section, elevated from bottom flange for $y_{G.C.}$=1.961 m. The QSS coefficient were compared in the table below, for wind tunnel tests and CFD analysis.

	Wind tunnel	**CFD**	**CFD**	**CFD**	**unit**
		no rails	with rails	Wind shields + rails	
C_d	0.681	0.572	0.661	0.525	-
C_l	-0.378	-0.057	-0.131	-0.065	-
C_m	-0.015	-0.020	-0.004	-0.008	-
$C`_d$	-0.009	0.019	-0.004	-0.004	1/deg
$C`_l$	0.057	0.078	0.066	0.060	1/deg
$C`_m$	0.017	-0.019	-0.017	-0.017	1/deg

Table: QSS coefficients for wind tunnel and CFD results for wind from west, K7-EndAnchored.

A reasonable match for drag C_d and for lift derivative $C`_l$ coefficients is observed in tale above. Other parameters are showing a similar tendency with some discrepancies. Discrepancy are observed for the lift coefficient and similar for all investigated cross sections. Optimal parameters found for this investigation are:

Parameters	**Value**
Wind speed	30m/s
Core size	0.1m
Time step	0.02s
Number of panels	400
Iteration number	1200

Table: Vortex panel method calculation parameters.

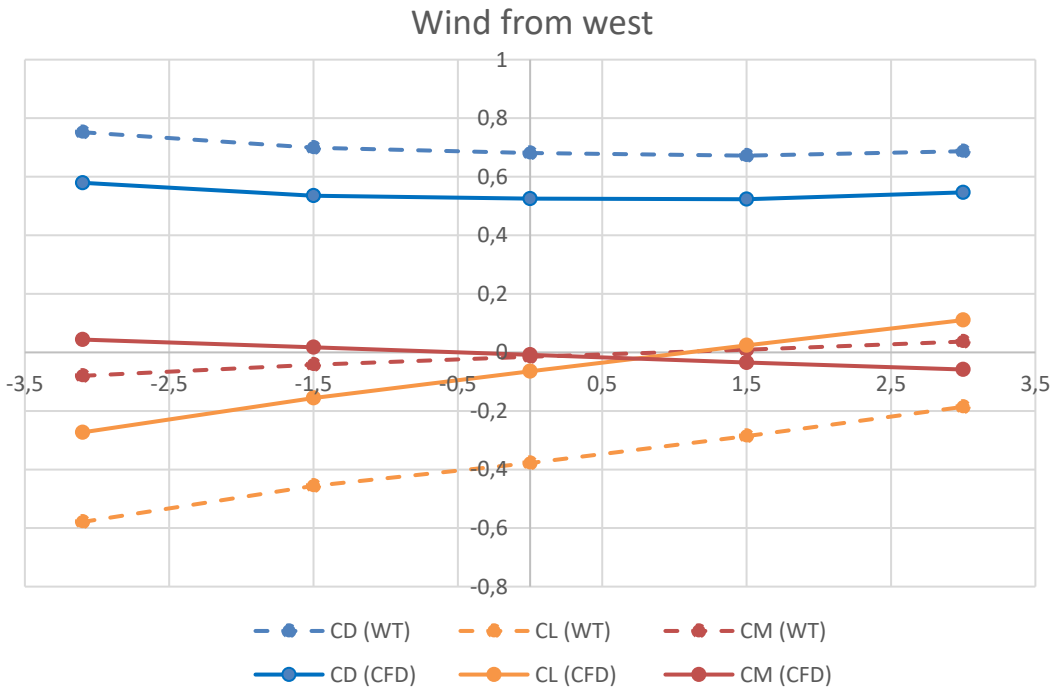

Figure: QSS derivatives compared between wind tunnel (dashed line) and CFD (full line), with side windshields - wind form west

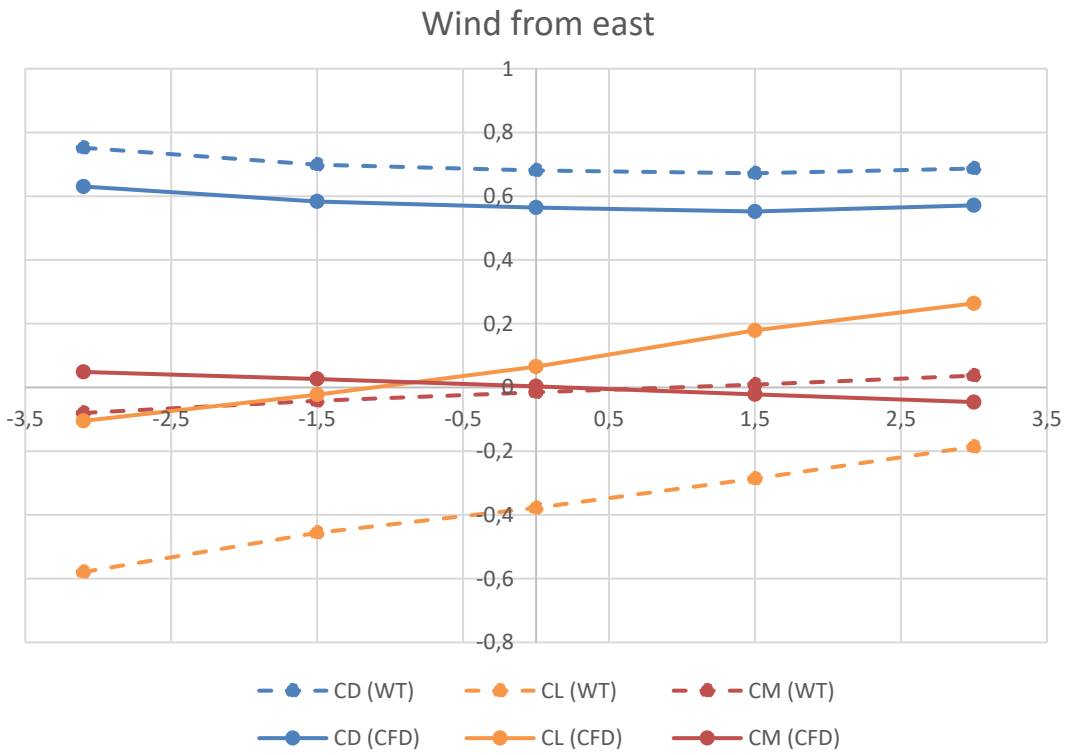

Figure: QSS derivatives compared between wind tunnel (dashed line) and CFD (full line), with side windshields – wind from the east.

Presented symmetric aerodynamic coefficients are showing the low influence of non-symmetric cross section. Therefore for further investigation are always considered for winds from the west.

Discussion on the difference of lift forces

Results were compared for wind tunnel tests without the boundary. In CFD analysis flow separation has an important influence on the pressure distribution and the lift coefficient. The analysis shows that flat nose separation is rather quick at the deck nose, causing a less favorable aerodynamic cross section. Lift coefficient cannot be exactly reproduced in the DVM method, due to boundary layer separation effects on the mean Cl coefficient. It is worth noting that Cl is consistent for different CFD models, but has larger uncertainties, therefore wind tunnel tests are taken as more reliable results. It is important to note that the wind tunnel results on lift force, show rather large lift force and might be due to some viscous effect commonly observed on small scale measurements. The CFD does not have similar viscus issues, however underlies boundary layer separation limitations. We suggest taking these effect and results into consideration in more detailed future investigations.
NOTE: Aerodynamic moment in RM has different sing convention as wind tunnel test results, where the moment is shown in different sign conventions.

Correction factor

Difference between wind tunnel measured forces and CFD lift force is expressed with a correction factor. This factor is then applied for proposed design values based on combined CFD and wind tunnel measurements results. This ensures the CFD investigation are calibrated with the wind tunnel tests. Keeping this relation to other CFD investigation, ensured possible reproduction of investigated cross sections in the wind tunnel experiment. With this approach we are achieving rather conservative design values in line with the wind tunnel test results.

Reliability of results

In conclusion, we can use calibrated CFD method to sufficiently accurately represent aerodynamic performance, drag force, lift derivative and moment force. The method is suited for relative comparisons between different windshields noses possibilities. It shows good agreement between wind tunnel tests and CFD results for drag C_d and for lift $C`_l$ coefficients. These two parameters have an important contribution to the floating bridge response.

2 Effects of wind shields and fences

Effect on different deck noses is investigated for different wind shield possibilities presented in Figure below:

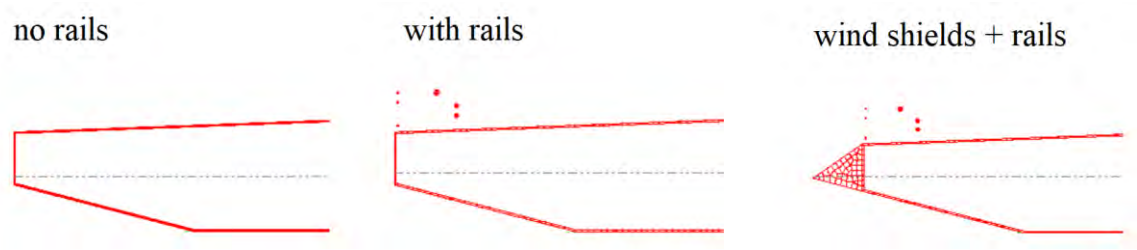

Figure: Parametric excitation.

The difference in aerodynamic performance is observed after introducing the wind shields. The drag coefficients reduce as well as the lift slope. This will lead to a lower global dynamic response of the floating bridge in both vertical and lateral direction.

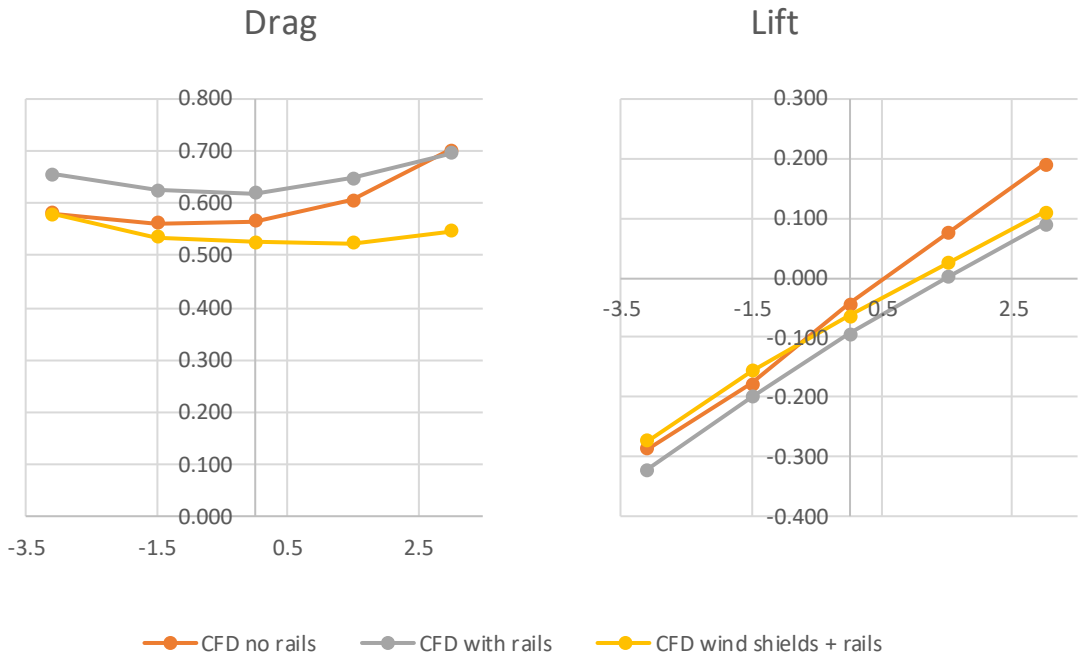

Figure: Comparing Aerodynamic performance for different cross sections.

Hence both fences with wind shields are important for final aerodynamic design and are therfore being included in further investigations.

3 Parametric investigation for improved aerodynamic design

Here investigated is cross section SS1 presented in Figure below.

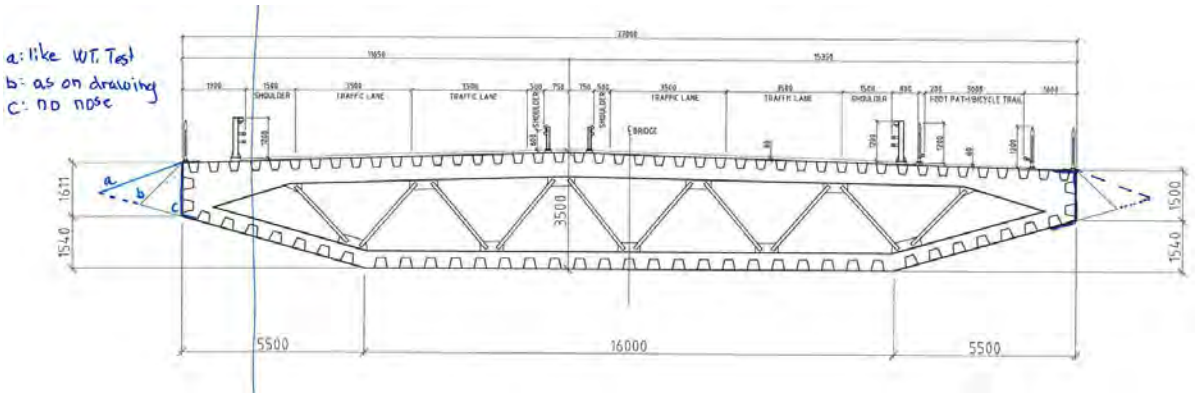

Figure: Investigated cross section SS1.

Investigated are five different cross-sections alternatives. On SS1-a is attached wind shield with width of 2m. CFD cross section is modeled with sharp corners and is expected not to have a significant effect on flow detachment. The SS1-b has attached 1m width wind shield, creating less sharp corner. The alternative SS1-c is without wind shields. Wind flow control is possible by introduction bottom attached wind guide. These are influencing the sooner reattaching the flow and are lowering vortex shedding force mechanism. The last alternative is round wind shield with a radius of about 0.82m was applied. All alternatives were investigated for a most suitable candidate for BJF 4 project, of side and end anchored bridge.

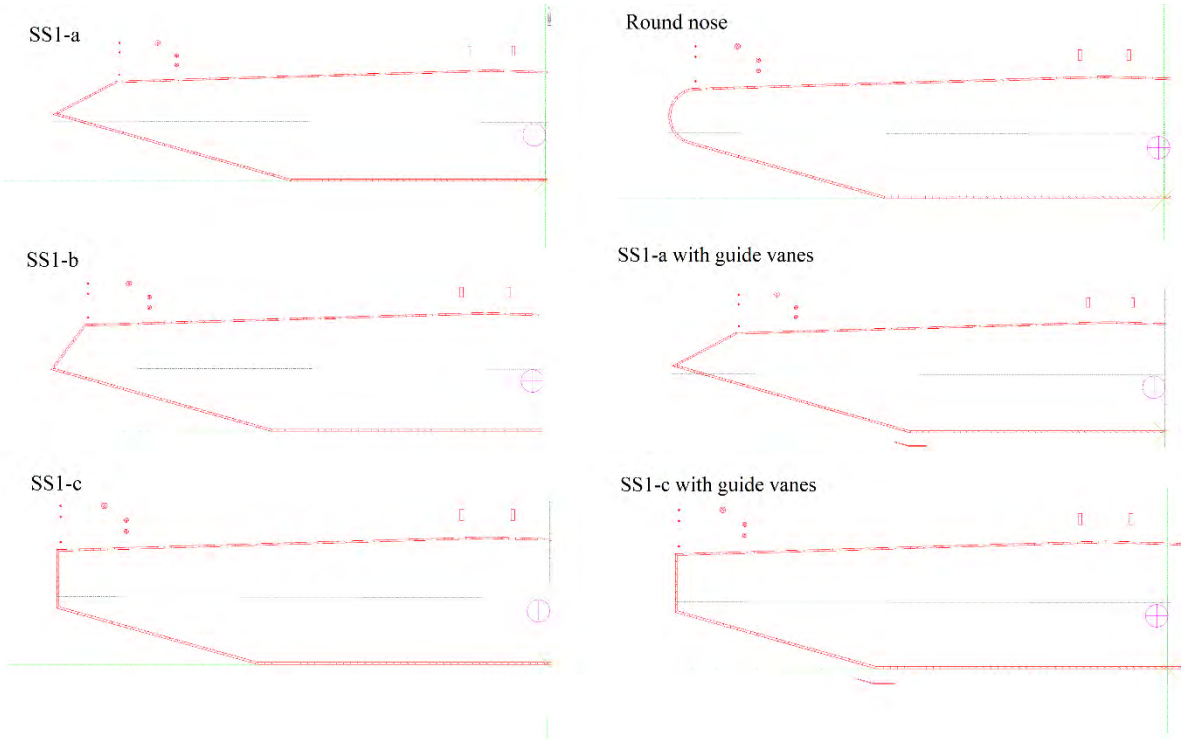

Figure: Different wind shields possibilities.

In order to find the optimal candidate, several parameters were compared. Sensitivities studies, taking into account the dynamics of the structure, showed that reduced drag coefficient will reduce horizontal response. Also lift angle derivative has an important influence on the vertical bridge response, therefore cross-section with lower lift angle derivative is preferable. Possible excessive vibrations of vortex shedding pattern should are being investigated. The aeroelastic performance of moving deck is investigated under smooth in the mean wind flow, presenting insight into aeroelastic response. Here following criteria were chosen to be evaluated for different wind shields, presented in table below.

PARAMETER	GOAL	RELEVANCE
Cd coefficient	Coefficient reduction	Important
Cl` derivative	Coefficient reduction	Important
Cm derivative	Coefficient reduction	Less important
Strouhal number	Informative	Vortex shedding
Flutter derivatives	Informative	Aeroelastic damping

Table: CFD investigation goals.

For six investigated cross section the drag forces are presented in Figure below. The low drag coefficient is achieved with the triangle wind shield nose, SS1-a and SS1-a with guide vane. These are the most suitable choices for obtaining low horizontal forces, during dynamic wind response.

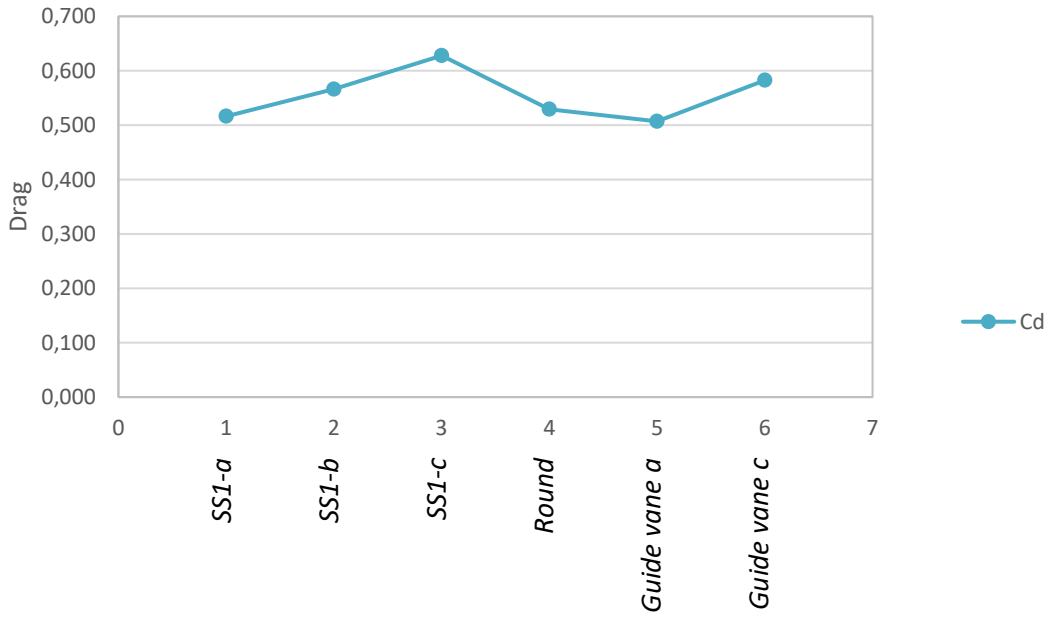

Figure: Drag aerodynamic coefficients.

The bending moment is increased for aerodynamic wind shields. The larger increment is observed for cross-section with sharp wind shield and guide vanes. For accurate compare, gravity centers should be properly considered. Bending moment are lower for rounded and less aerodynamic cross section SS1-b, SS1-c.

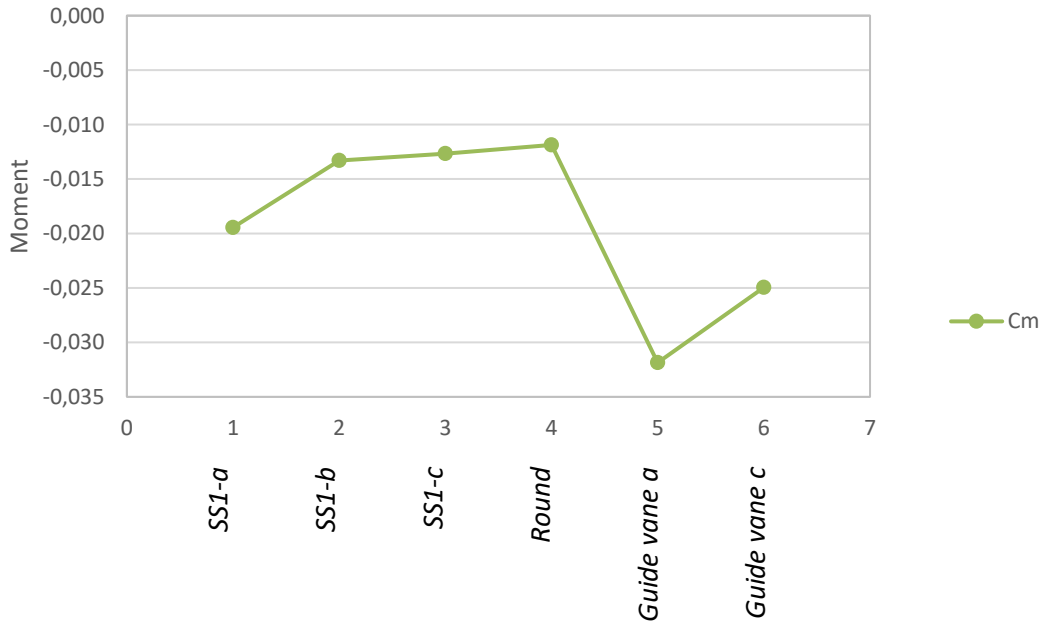

Figure: Moment aerodynamic coefficients.

The lift and angle derivative are important contribution to the vertical response of the bridge. Important reduction of lift coefficients is achieved by the introduction of wind shields. Even more significant reduction is achieved when installing guide vanes. This helps with wind flow reattachment making cross-section less sensitive to the angle variation and is in this category the most suitable candidate.

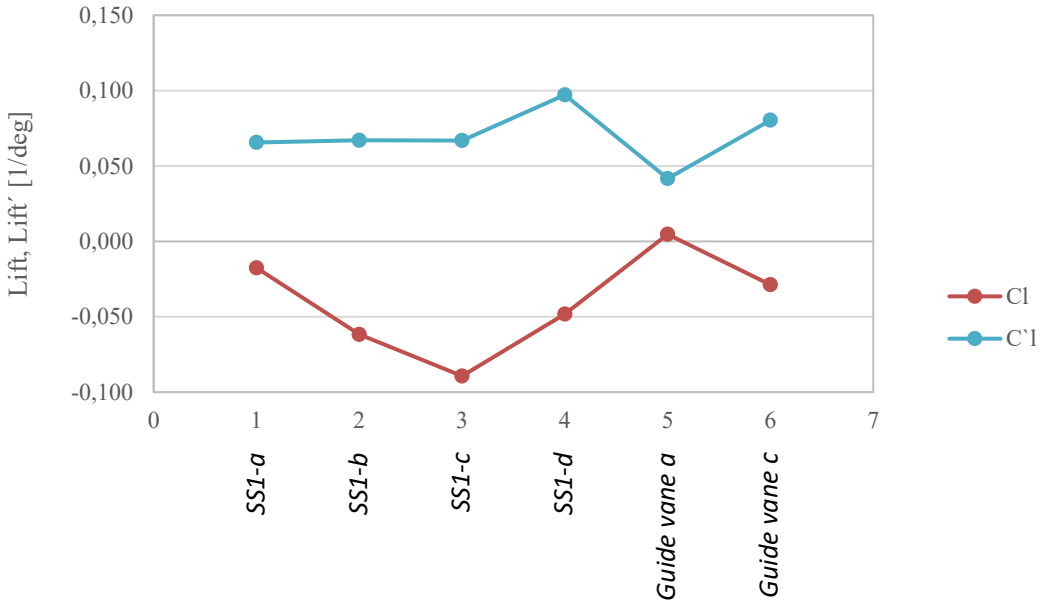

Figure: Lift and their angle derivative aerodynamic coefficients.

A more comprehensive and accurate aerodynamic performance can be achieved by analysis also different vertical wind angles. In this investigation following angles were investigated for following angle

$$Vertical\ angles = [-12, -8, -5, -3, -1.5, 0\ ,1.5, 3, 5, 8, 12]$$

and can be depicted in Figure below.

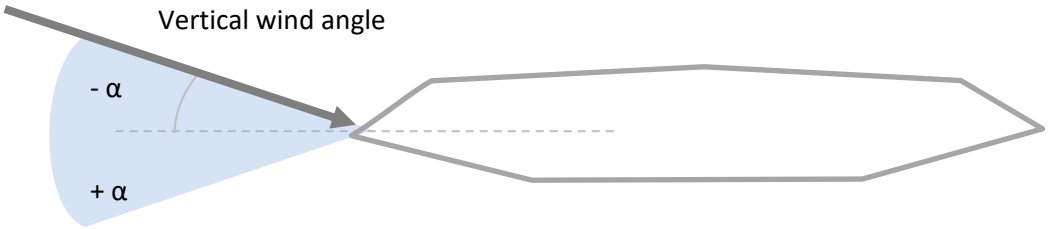

Figure: Vertical wind angles.

The lift derivative is presented for investigates a range of angles in Figure below. Preferred are coefficients with low values and showing constant for investigated vertical angles. The analysis shows that round wind shield is strongly variating and can result in unvented dynamic effects. The cross sections with guide vane cross-section show an optimal low coefficient for different angles of attack. This would suitable candidate due to their low constant coefficients. The wind flow with guide vanes is more constant linearized and will support best the linearization assumptions of turbulent wind dynamic calculations.

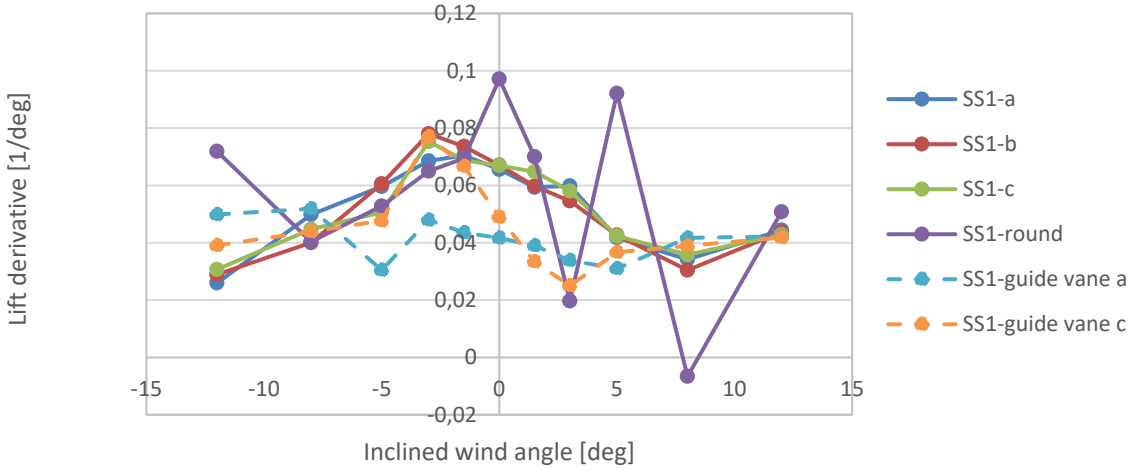

Figure: Lift angle derivative coefficient for different vertical wind angles.

Further investigated is aerodynamic stability, such as vortex shedding, galloping and flutter in below section.

The estimation of vortex shedding frequency can be expressed through normalized Strouhal number defined by:

$$St = \frac{fB}{V}$$

This expresses oscillating forces for selected wind regime. It is Reynolds number dependent and is Re=10e4 for this CFD analysis. In this investigation different noses have an influence on the shedding oscillations and are presented in table below.

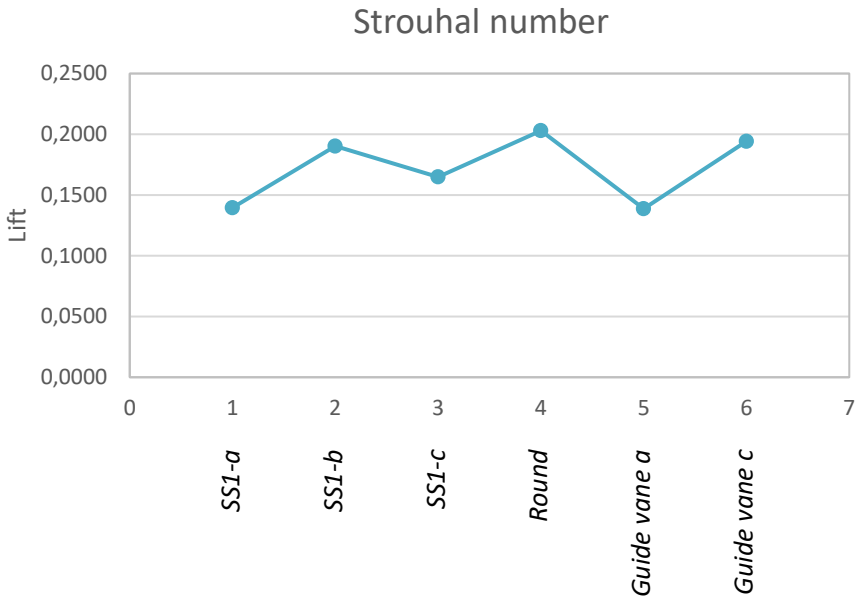

Figure: Strouhal number for vertical.

Presented results are for the time series of vortex shedding lift force. Main vortexes can be observed for SS1-c at frequency 1Hz. By installing the wind guides the main oscillation frequency moves for SS1-c with wind guides from 1.0 Hz to 1.2Hz. The RMS of lift forces is reduced. This leads to a vortex shedding at higher velocity and will forces lover vortex shedding vibrations. The installation of wind guides has been investigated for alternatives SS1-a for an aerodynamic cross-section with wind shields and SS1-c for aerodynamic cross section without wind shields. Vortex-induced lift force results are summaries in table below:

	SS1-a Aerodynamic cross section with wind shield		**SS1-c** Aerodynamic cross section	
	no guide vanes	with guide vanes	no guide vanes	with guide vanes
Main frequency [Hz]	1.3	0.9	1.4	1.0
RMS [kN]	2.5	1.9	2.6	2.3
Mean [kN]	1.0	1.1	2.5	2.3

Table: Lift vortex shedding force calculated in CFD analysis.

From table above following observation can be made. The installation of wind shields and wind guides have important impact on vortex shedding pattern. The reduction of vortex shedding force mechanism is best achieved by installing the wind guides together with wind shields. This will increase shedding frequency and reduce the lift oscillation for about 30%. This will result in possible lover vortex shedding vibrations. Since vortex shedding vibrations are typical low wind regime phenomenon, the shift in oscillation frequency can disrupt vortexes formation. Installation of wind shields results in lover RMS lift forces, this in case of locked-in will lead to lover vibrations. To achieve the disruption of the vortex shedding vibration a proper design of wind guides must be considered, not all wind guides will achieve wanted effects.

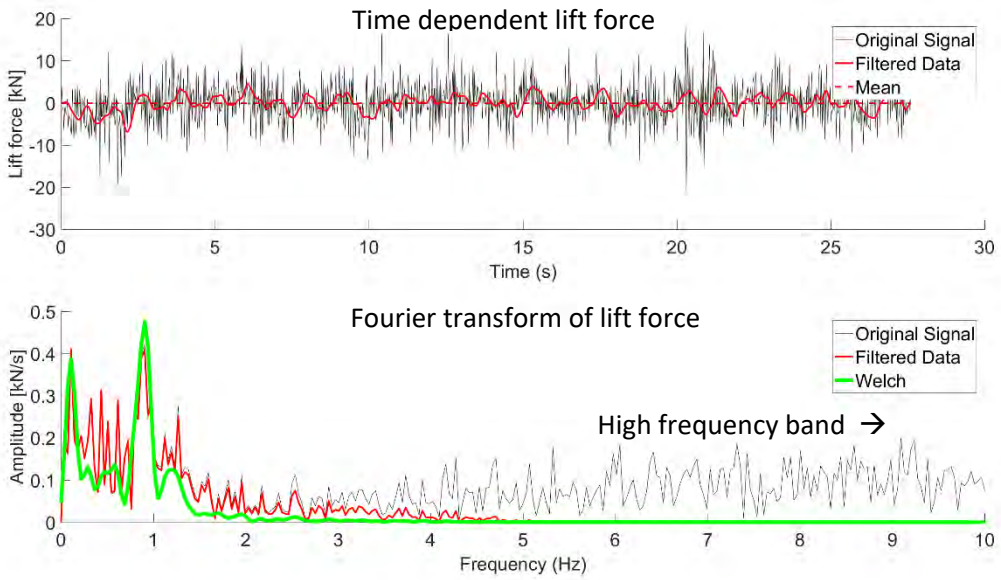

Figure: Time series and Fourier transform of lift force, for SS1-c.

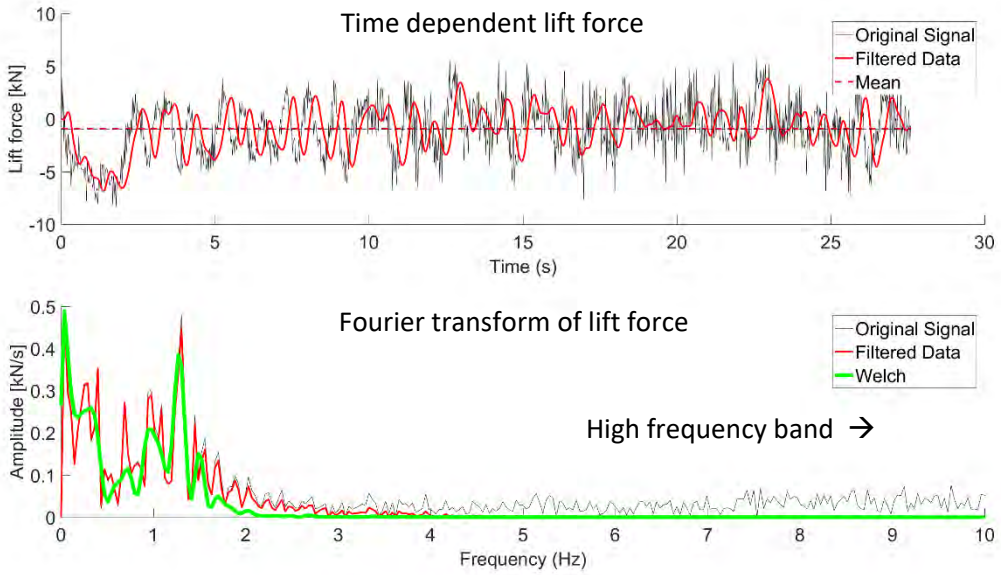

Figure: Time series and Fourier transform of lift force, for SS1-c with wind guides.

Here different deck noses are investigated for galloping criteria. The one DOF galloping is evaluated for Glauert-Den Hartog criterion for galloping, defined by negative values of the lift values $(C`_L + C_D) > 0$. Higher values of expression in round brackets exclude possibility of low wind speed galloping instability.

This criterion shows unstable cross sections for negative values and is presented for different noses in figure below. The round wind shield cross section is not aerodynamically stable and is not be suitable for this crossing. Other cross sections are showing stable galloping design.

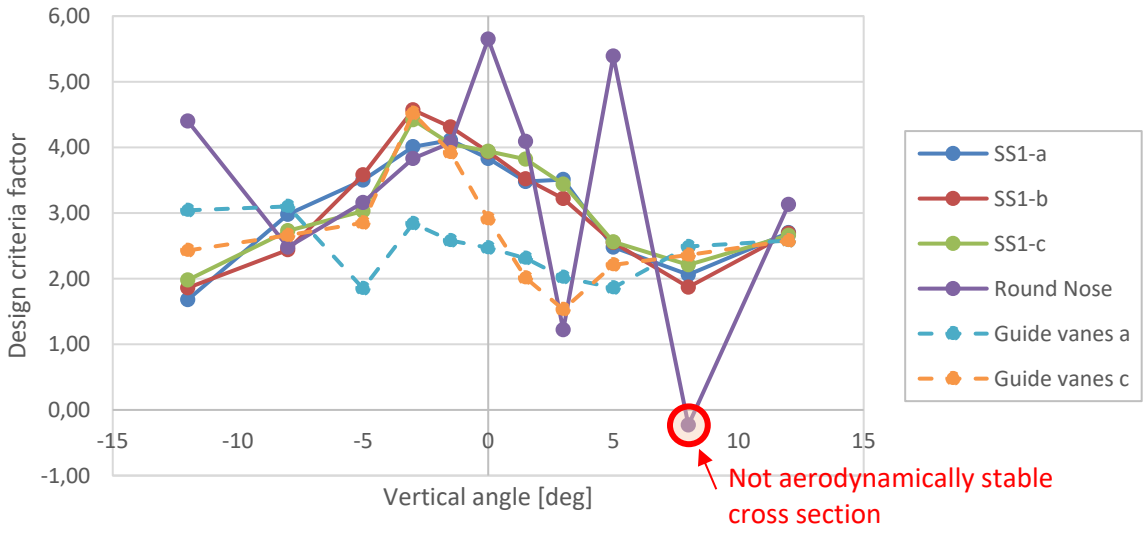

Figure: Galloping design criteria.

The results were normalized on reference cross section SS1-a, with torsional divergence wind speed about 120m/s. The normalization is performed in order to observe a relative difference compared to the initial proposed SS1-a. All values are still well above the instability tolerance of 82m/s, see report: See 08-NOT-176 Aerodynamic Stability. Dynamic torsional divergence is presented for a single torsional DOF instability in presented I Figure below:

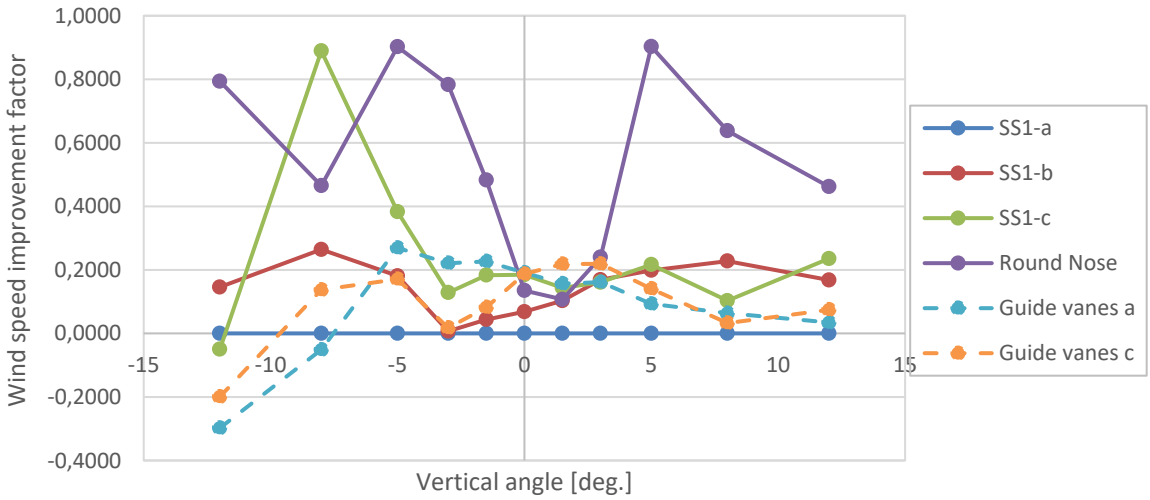

Figure: Normalized torsional divergence wind speed factor.

Flutter derivatives extraction validation

Additional internal FSI validations were also conducted on similar cross-sections and compared to WT. With calibration process is possible to achieve excellent agreements for aerodynamic 2D cross sections, for flutter derivatives in vertical and torsional direction. We run FSI with a different set of calibration parameters, tailored for flutter extraction, overall, they provide very reliable results.

Additional test on flutter derivatives on a reference bridge was performed and found that they give reasonable flutter onset speed. See 08-NOT-176 Aerodynamic Stability.

Flutter derivatives extraction validation

Flutter derivatives are extracted with force vibration FSI techniques. Results are presented for most important aeroelastic damping flutter derivatives in vertical H1* and horizontal direction A2*. The results are plotted in the format of reduced Frequency K on the horizontal axis and flutter derivatives are multiplied with K on a vertical axis. This allows for a better overview of QSS participation and their frequency contribution. Aeroelastic investigation shows similar results for all candidates. Higher damping in vertical DOF is observed for SS1-guide vanes, what will result in higher damping of vertical vibrations. This will lead to a lower global response in the vertical direction for present mean wind. Low vertical and torsional damping are showing SS1-c and SS1-round nose.

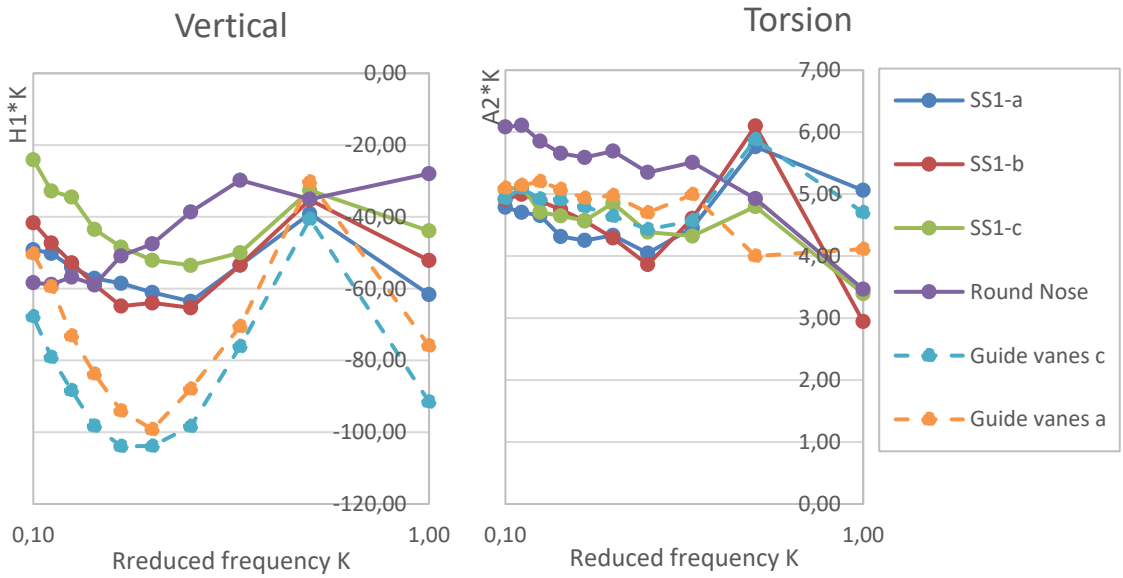

Figure: Flutter derivative for vertical and torsional damping.

The floating bridge has main contribution to vertical response are periods around T=7s. Vertical damping was calculated for wind speed V=25m/s for lift response and is shown in Figure below:

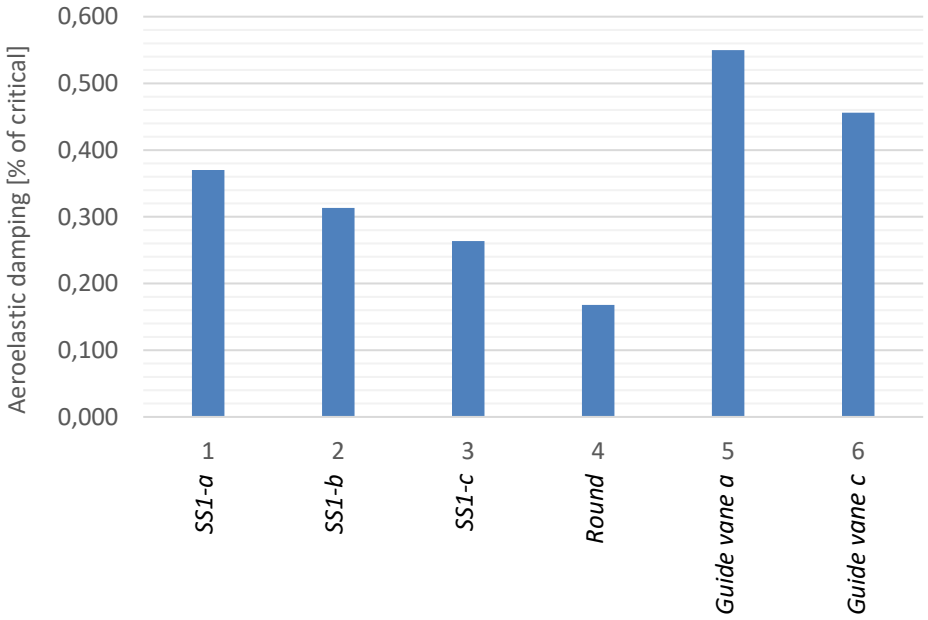

Figure: Present of critical vertical damping for V=25m/s and T=7s.

4 Proposed design values

Here proposed are different aerodynamic coefficients combined from wind tunnel tests and CFD analysis. The results are conservative values for vertical angles [-8 and + 8] and are listed in table below:

	SS1-a			SS1-c		
Angle	Cd	Cl	Cm	Cd	Cl	Cm
[deg]	[]	[]	[]	[]	[]	[]
-8	1.261	-0.941	0.110	1.538	-1.062	0.077
-5	0.883	-0.731	0.069	1.093	-0.873	0.061
-3	0.752	-0.579	0.033	0.910	-0.748	0.037
-1.5	0.699	-0.456	0.007	0.851	-0.661	0.010
0	0.681	-0.378	-0.019	0.828	-0.536	-0.013
1.5	0.672	-0.286	-0.045	0.841	-0.397	-0.039
3	0.687	-0.186	-0.067	0.862	-0.263	-0.061
5	0.766	-0.073	-0.096	0.938	-0.133	-0.086
8	0.909	0.052	-0.125	1.074	0.000	-0.118

Table: Design values for BJF Phase 4 project, cross section SS1-a and SS1-c.

These results are based on calibrated wind tunnel tests and extrapolated CFD investigations. Present is an envelope of most unfavorable results used for the design. The CFD had rather distinctive results on Cl, however very consistent when comparing different methods. The difference between CFD / WT results in a factor for lift component. This factor has been used to scale up the other alternatives calculated by CFD.

In other words, we trust Cl more to the wind tunnel results, so we are taking them over. With this approach, we are achieving rather conservative WT design values.

5 Conclusion

Different wind noses were investigated for aerodynamic performance. Based presented CFD results combined with the criteria for this project, the following conclusion can be made:

- Aerodynamic design is improved by introducing the wind shields. Statical and dynamic wind performance are improved.

- Aerodynamic design can be fouther improved by installation of guide vanes at the bottom of the cross-section. This reduces the flow detachments resulting in a more constant linearised aerodynamic properties. This investigation shows that quasi-static, vortex shedding and aeroelastic performance are improved.

- From six investigated cross-section, the most goal suitable SS1-c with guide vane cross section was found. The second pace is SS1-a with guide vane cross-section. Other cross sections are showing less optimal aerodynamic performance and will lead to a higher global response of the floating bridge.

- Round wind shield section is not aerodynamically stable and therefore is not recommended for application in this project.

6 References

/1/ SBJ-32-C4-SVV-90-BA-001 - Design Basis Bjørnafjorden. Rev 0.

/2/ SBJ-32-C4-SOH-20-RE-001 - Wind model testing for floating bridge, small-scale test, step 1

/3/ NS-EN 1991-1-4:2005+NA:2009. Eurocode 1: Action on structures. Part 1-4: General actions – Wind actions

/4/ 08-NOT-60_00_AerodynamicLoadCoeffSensitivity.pdf

/5/ 08-NOT-xx_00_AerodynamicLoadCoeffSensitivity_20190208.pdf

/6/ Theory of Bridge Aerodynamics, Einar Strømmen, 2010

/7/ Wind OnDemand, Matlab Scripts for vortex shedding analysis, 2017-2019

AAS-JAKOBSEN COWI Multiconsult

JOHS HOLT AkerSolutions entail NGI DISSING+WEITLING architecture a|s mossmaritime

Concept development, floating bridge E39 Bjørnafjorden

Appendix E – Enclosure 6

10205546-08-NOT-068

Buffeting effects of inhomogeneity

MEMO

PROJECT	**Concept development, floating bridge E39 Bjørnafjorden**	DOCUMENT CODE	10205546-08-NOT-068
CLIENT	Statens vegvesen	ACCESSIBILITY	Restricted
SUBJECT	**AMC status 2 – Buffeting effects of inhomogeneity**	PROJECT MANAGER	Svein Erik Jakobsen
TO	Statens vegvesen	PREPARED BY	Allan Larsen
COPY TO		RESPONSIBLE UNIT	AMC

SUMMARY

This memo summarizes an evaluation of the effects of inhomogeneities of the wind field on the gust response of the K11 floating bridge.

It is concluded that the constant longitudinal mean wind speed profile results in the highest wind loading. Also it is concluded that the different percentiles for the turbulence parameters produces the highest turbulence loading in different frequency intervals. The frequency intervals are identified for horizontal and vertical turbulence.

0	29.03.2019	Status 2 issue	A. Larsen	K. Aas-Jakobsen	S. E. Jakobsen
REV.	DATE	DESCRIPTION	PREPARED BY	CHECKED BY	APPROVED BY

1 Introduction

The Design Basis for the Bjørnafjorden crossing /1/ specifies variations of the horizontal mean wind profile for winds perpendicular to the bridge line. Further the Design Basis also proposes a statistical variation the turbulence properties. This memo summarises a dynamic wind response analysis aiming at clarifying the effect of the inhomogeneities of the wind field on the buffeting (gust) response of the Bjørnafjorden floating bridge.

2 Analysis model

The analysis presented applies Davenports statistical frequency domain gust response analysis which is applicable to "line like" structures /3/. Thus, possible effects of the horizontal curvature of the bridge deck are neglected assuming that the wind is everywhere perpendicular to the bridge line.

3 Wind field

The Design Basis /1/ specifies the inhomogeneity for the wind field as discussed below.

3.1 Mean wind field

The variations of the mean wind speed V along the bridge line may assume three along line distributions as follows:

1. Constant
2. Lineary varying form $0.6 \cdot V$ at one end to V on the other.
3. Lineary varying from $0.8 \cdot V$ at one end to V in the middle to $0.8 \cdot V$ on the other end.

Combining the above along line distributions with mean wind variation with height as described by the N400 vertical logarithmic wind profile yields the along line mean wind distributions shown in Figure 3.1.

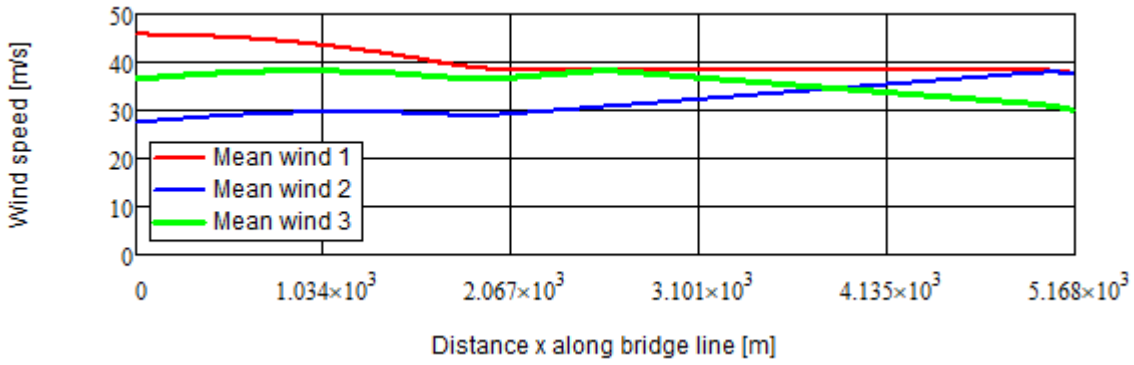

Figure 3.1 Mean wind distributions $V(x)$ along the Bjørnafjorden bridge line.

A 10 min. basis wind speed V_b = 30.5 m/s has been applied assuming a 50 year return period following /1/ Table 12.

3.2 Turbulence properties

The standard deviations $\sigma_{u,w}$ of the along wind and vertical components of the turbulent wind field will vary along the bridge line due to the change in elevation of the bridge girder and due to the three mean wind profiles as described above. Apart from this the length scales L_u^x, L_w^x and spectral density coefficients A_u, A_w appearing in the power spectral densities (PSDs) of the wind and the

decay constants C_{yu}, C_{yw} appearing in the root coherences have been assigned varying values depending on their probabilities of occurrence, /1/, Table 15.

In general the length scales of turbulence are expected to be a function of the level z above ground. N400 /2/ specifies the following functional relationship:

$$L_u^x(z) = 100\left(\frac{z}{10}\right)^{0.3} \tag{1}$$

Which assumes L_u^x = 100 m at reference height z = 10 m.

To apply the length scales given in /1/ Table 15 directly, the reference height is changed to z = 50 m yielding:

$$L_u^x(z) = 100\left(\frac{50}{10}\right)^{0.3}\left(\frac{z}{50}\right)^{0.3} = 162\left(\frac{z}{50}\right)^{0.3} \tag{2}$$

As the level of the bridge girder is a function of the along line coordinate the length scales will also be functions of the along line coordinate x, Figure 3.2.

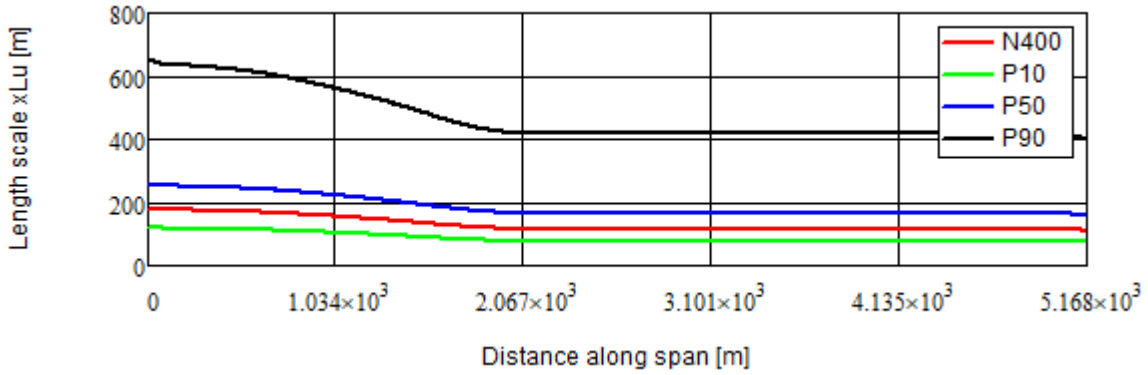

Figure 3.2 Variation of the length scale L_u^x as function of the along line coordinate and assigned probabilities of occurrence.

The decrease in length scale with increasing along line coordinate reflects the decreasing level of the bridge girder as the bridge progresses from the high-level cable stayed bridge into the floating spans.

For the present analysis the velocity power spectra $S_{u,w}(x,n)$ and root coherences $\gamma_{u,w}(x_1,x_2,n)$ along the bridge line are modelled as follows:

$$S_{u,w}(x,n) = \frac{\left(I_{u,w}(x)V_{p(x)}\right)^2 A_{u,w}\dfrac{L_{u,w}^x(x)}{V_{p(x)}}}{\left(1+1.5A_{u,w}\dfrac{nL_{u,w}^x(x)}{V_{p(x)}}\right)^{5/3}} \tag{3}$$

$$\gamma_{u,w}(x_i,x_j,n) = exp\left(\frac{-C_{yu,yw}\left|x_i-x_j\right|n}{\left(\dfrac{V_p(x_i)+V_p(x_j)}{2}\right)}\right) \tag{4}$$

Where $V_p(x)$ is the longitudinal mean wind distribution (p = 1, 2,3), Figure 3.1, x_i, x_j are positions on the bridge line and n is the frequency in Hz.

Plots of the along wind (u) power spectra made non-dimensional by division with the mean wind squared and root coherences for N400 and the 10, 50 and 90 percentiles are presented in Figure 3.3, Figure 3.4 below.

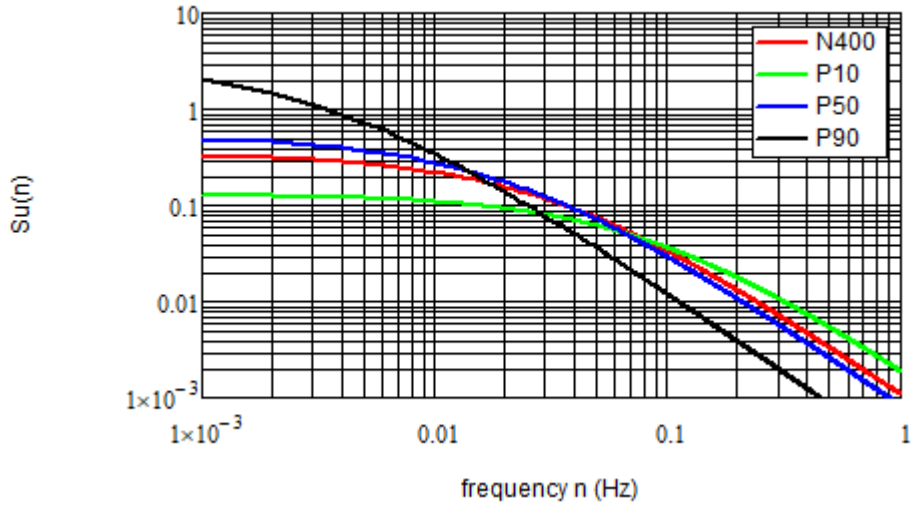

Figure 3.3 Non-dimensional along wind power spectra following N400 and 10, 50 and 90 percentiles /1/. Reference height z = 16.3 m corresponding to the level of the floating spans.

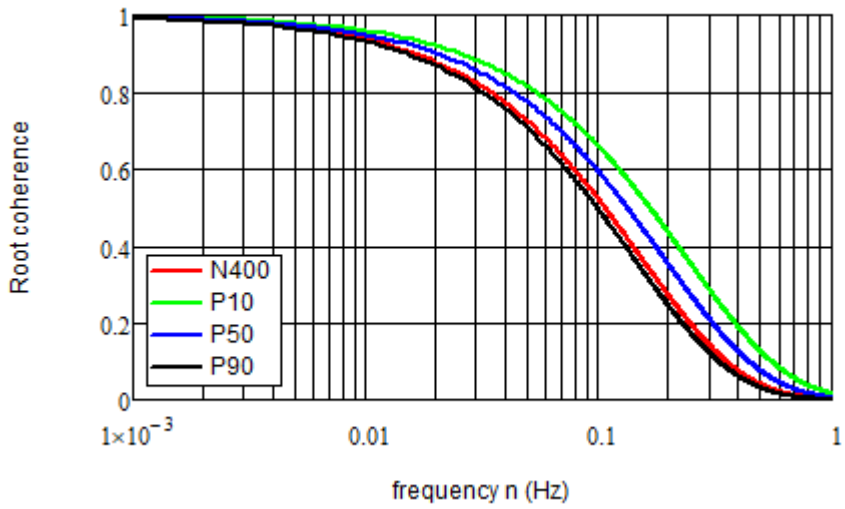

Figure 3.4 Along wind root coherences following N400 and 10, 50 and 90 percentiles /1/. Reference length corresponding to one deck width B = 30 m.

The power spectra in Figure 3.3 indicate that the turbulent wind loading appear to be largest following the P90 assumption for frequencies below 0.015 Hz. The N400 or P50 assumptions appear to yield the largest wind loading in the mid frequency range 0.015 Hz to 0.06 Hz whereas the P10 assumption yields the largest loadings at frequencies above 0.06 Hz.

It is possible to derive a formula for the cross over frequency between the different frequency ranges yielding the highest wind assuming that the wind loading along the entire bridge line is dominated by the loading at a certain height, say the deck level z = 16.3 m of the floating spans:

$$n_x = \frac{U_{16.3}}{1.5}\left[\frac{(A_{u2}L_{u2}^x)^{3/5} - (A_{u1}L_{u1}^x)^{3/5}}{(A_{u2}L_{u2}^x)(A_{u1}L_{u1}^x)^{3/5} - (A_{u1}L_{u1}^x)(A_{u2}L_{u2}^x)^{3/5}}\right] \quad (5)$$

Where $L_{u1}^x A_{u1}$ and L_{u2}^x, A_{u2} are the length scales and spectral density constants associated with the low frequency and high frequency percentile spectra respectively. Inserting the appropriate

spectral parameters in (5) yields the first cross over frequency between the 90 and 50 percentile range as n_{x1} = 0.014 Hz and the second cross over frequency between the 50 and 10 percentile range as n_{x2} = 0.065 Hz. Both in agreement with Figure 3.3.

3.3 Total gust loading due to horizontal along wind turbulence

The above conclusion regarding cross over frequencies may be slightly distorted by the root coherence which yields the highest coherence of the turbulence following the P10 assumption and the least coherence for the P90 assumption.

The combined influence of the power spectral parameters L_u^x, A_u and the coherence decay constant C_{yu} can be accessed via the spectrum of the integral horizontal turbulent loading (gust) along the bridge line:

$$Q(n) = \int_0^L \int \sqrt{\left(C_D B V_p(x_i) \right)^2 S_u(x_i, n) \left(C_D B V_p(x_j) \right)^2 S_u(x_j, n)}\, \gamma_{u,w}(x_i, x_j, n)\, dx_i dx_j \qquad (6)$$

$Q(n)$ is made non-dimensional by division with the integral mean turbulent wind loading $\left(\rho B C_D \int_0^L I_u(x) V_p(x)^2 dx\right)^2$ and plotted in Figure 3.5.

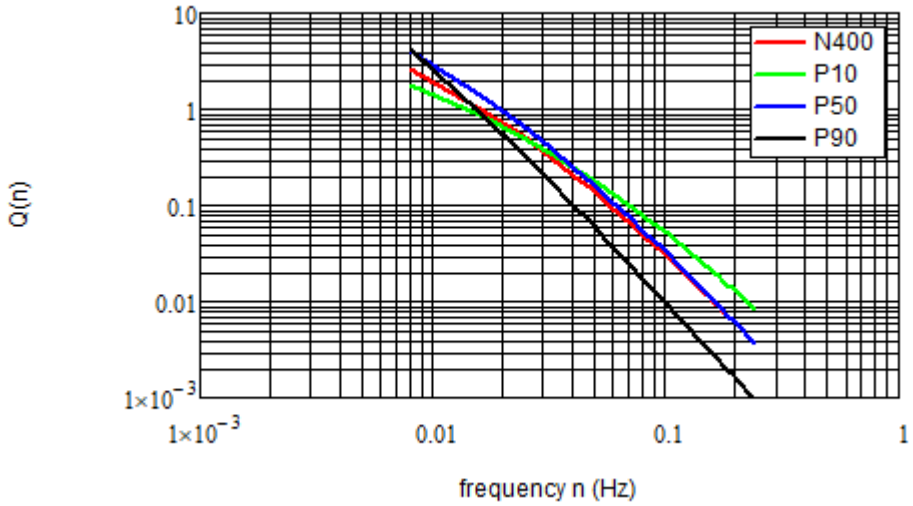

Figure 3.5 Non-dimensional along wind integral turbulent wind loading on the bridge line.

Figure 3.5 displays slightly lower cross over frequencies than predicted from (5) likely due to the influence of the higher levels of the cable stayed bridge. In general, Figure 3.5 supports the notion that the P90 parameters yield the largest along wind effects at very low frequencies less than 0.01 Hz. The P50 parameters yield the largest effects in in the frequency range 0.01 Hz – 0.035 Hz and that the P10 parameters yield the largest effects at frequencies above 0.05 Hz.

3.4 Total gust loading due to vertical turbulence

The above considerations refer to the along wind (u) turbulence which relates to the low frequency horizontal motions. Vertical and torsion motions occur at frequencies which are typically one magnitude higher and are excited mainly by the vertical (w) turbulence. A plot of the non-dimensional vertical gust loading applying the relevant length scales, spectral density constants and decay constants is shown in Figure 3.6.

It is noted that that the P90 and P50 parameters yield the largest and almost similar vertical wind loading at 0.1 Hz. The P50 parameters yield the largest effects in the frequency range 0.1 Hz – 0.35 Hz and that the P10 parameters yield the largest effects at frequencies above 0.35 Hz. It is also

noted that the differences in the non-dimensional loadings for the different percentiles are less than for the horizontal turbulence.

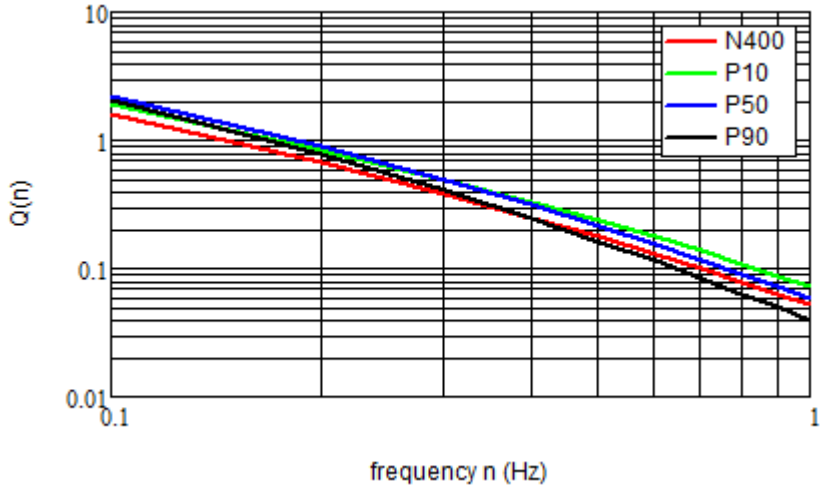

Figure 3.6 Non-dimensional vertical integral turbulent wind loading on the bridge line.

4 The Davenport gust response model

Following Davenport /3/ the two-point along wind turbulent loading $Q_{uu}(x_i, x_j, n_m)$ at the eigenfrequency n_m is obtained by combining turbulent power spectra and root coherences as follows:

$$Q_{uu}(x_i, x_j, n_m) = \sqrt{\left(C_D B V_p(x_i)\right)^2 S_u(x_i, n_m) \left(C_D B V_p(x_j)\right)^2 S_u(x_j, n_m)}\, \gamma_u(x_i, x_j, n_m) \quad (7)$$

The standard deviation of the maximum modal response due to turbulence, say in the horizontal direction y, is the obtained by integrating $Q_{uu}(x_i, x_j, n_m)$ and mode shape over the length of the bridge line and dividing by modal mass:

$$\sigma_y = \sqrt{\frac{\frac{\pi n_m}{4\zeta_m} \iint_0^L Q_{uu}(x_i, x_j, n_m) \varphi_m(x_i) \varphi_m(x_j) dx_i dx_j}{(2\pi n_m)^4 M_m^2}} \quad (8)$$

Where n_m, M_m, ζ_m is eigenfrequency, modal mass and modal damping of the $m'th$ mode having mode shape $\varphi_m(x)$ along the bridge line. L signifies the total length of the bridge.

The modal damping ζ_m is obtained as the sum of two contributions, the structural damping ζ_s and the aerodynamic damping ζ_a. The aerodynamic damping depends on the mean wind speed, the modal mass and aerodynamic load coefficient as follows:

$$\zeta_a = \frac{\frac{\rho B C_D}{L} \int_0^L V_p(x) dx}{4\pi n_m \frac{M_m}{\int_0^L \varphi_m(x)^2 dx}} \quad (9)$$

Where C_D is the drag coefficient normalized by deck width B.

In case the standard deviation of the vertical maximum modal response σ_z is to be calculated, C_D is to be replaced by ½ times the lift slope C_L' and $S_u(x, n_m)$ by $S_w(x, n_m)$ in (7), (9). The appropriate vertical mode shapes are to be applied in (3) instead of horizontal mode shapes.

(7), (8), (9) can only be evaluated for certain simplified assumptions of contributing mode shapes and mean wind distributions /3/. In the present case (7), (8), (9) are evaluated numerically.

5 Numerical example

Evaluation of structural responses following (8) for different modes and eigenfrequencies is carried out with a view to support the general conclusion arrived at in section 3. The gust response analysis is based on modal properties for the K11 end anchored bridge developed 08-02-2019 assuming wind perpendicular to the bridge line.

Parameters related to the K11 end anchored bridge are chosen as follows:

Air density ρ = 1.25 kg/m^3

Deck width B = 30 m

Total bridge length L = 5168 m

Drag coefficient (horizontal along wind modes) C_D = 0.1

Lift slope (vertical cross wind modes) C_L' = 3.87

Structural damping ζ_s = 0.005

5.1 Horizontal mode 1

The first horizontal (along wind) mode of the bridge represents an almost sinusoidal wave along the bridge line, Figure 5.1. The eigenfrequency and modal mass is obtained from FEM analyses as : n_1 = 0.0088 Hz and M_1 = 94828·10^3 kg.

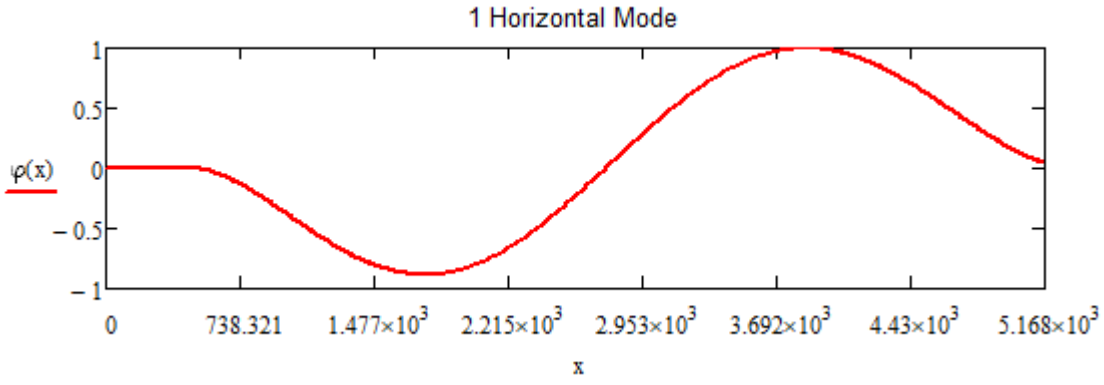

Figure 5.1 Mode shape of first horizontal mode of K11 end anchored bridge.

The maximum modal response σ_y for horizontal wind profiles 1, 2,3 and the specified variations of the turbulence parameters are presented in Table 5.1.The upper part of the table reproduces the variation of the turbulence parameters specified in the Design Basis. The lower part of the table gives the calculated standard deviation of the maximum modal responses as function of turbulence parameters and horizontal mean wind profile as described in section 3.1.

Table 5.1 Standard deviations of maximum modal responses for horizontal mode 1.

Mode	N400	P10	P50	P90
1. Horizontal n_1 = 0.0088 Hz	L_u^x = 162 m	L_u^x = 108 m	L_u^x = 232 m	L_u^x = 586 m
	A_u= 6.8	A_u= 3.9	A_u= 7.3	A_u= 16.3
	C_{yu} = 10.0	C_{yu} = 6.4	C_{yu} = 8.0	C_{yu} = 10.8
Wind 1	σ_y = 5.14 m	σ_y = 3.96 m	σ_y = 6.16 m	σ_y = 6.53 m
Wind 2	-	σ_y = 3.56 m	σ_y = 5.63 m	σ_y = 5.58 m
Wind 3	-	σ_y = 3.82 m	σ_y = 5.83 m	σ_y = 5.98 m

5.2 Horizontal mode 2

The second horizontal (along wind) mode of the bridge represents an almost sinusoidal 1½ wave shape along the bridge line, Figure 5.2. The eigenfrequency and modal mass is obtained from FEM analyses as: n_2 = 0.0166 Hz and M_2 = 54174·10^3 kg.

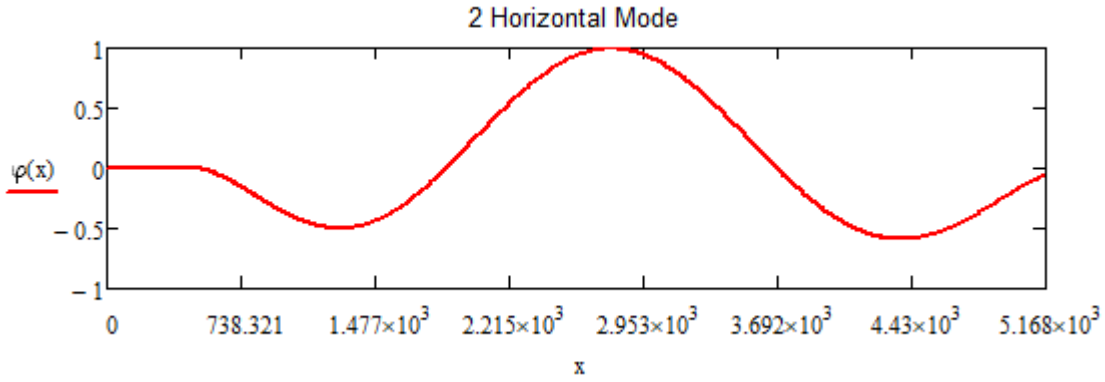

Figure 5.2 Mode shape of second horizontal mode of K11 end anchored bridge.

The maximum modal response σ_y for horizontal wind profiles 1, 2,3 and the specified variations of the turbulence parameters are presented in Table 5.2 below.

Table 5.2 Standard deviations of maximum modal responses for horizontal mode 2.

Mode	N400	P10	P50	P90
2. Horizontal n_2 = 0.0166 Hz	L_u^x = 162 m	L_u^x = 108 m	L_u^x = 232 m	L_u^x = 586 m
	A_u= 6.8	A_u= 3.9	A_u= 7.3	A_u= 16.3
	C_{yu} = 10.0	C_{yu} = 6.4	C_{yu} = 8.0	C_{yu} = 10.8
Wind 1	σ_y = 2.26 m	σ_y = 1.94 m	σ_y = 2.62 m	σ_y = 2.45 m
Wind 2	-	σ_y = 1.77 m	σ_y = 2.26 m	σ_y = 1.79 m
Wind 3	-	σ_y = 1.93 m	σ_y = 2.56 m	σ_y = 2.12 m

By comparing Table 5.1 and Table 5.2 it is noted that the response of mode 1 for P90 assumes the largest value where as the response for mode 2 assumes the largest value for P50 as is expected from the considerations in section 3. A similar trend is observed for mode 10, Table 5.3, where P10 produces the largest responses.

5.3 Horizontal mode 10

The 10th horizontal (along wind) mode of the bridge represents an almost sinusoidal 4 wave shapes along the bridge line. The eigenfrequency and modal mass is obtained from FEM analyses as: n_{10} = 0.1155 Hz and M_{10} = 34273·10^3 kg.

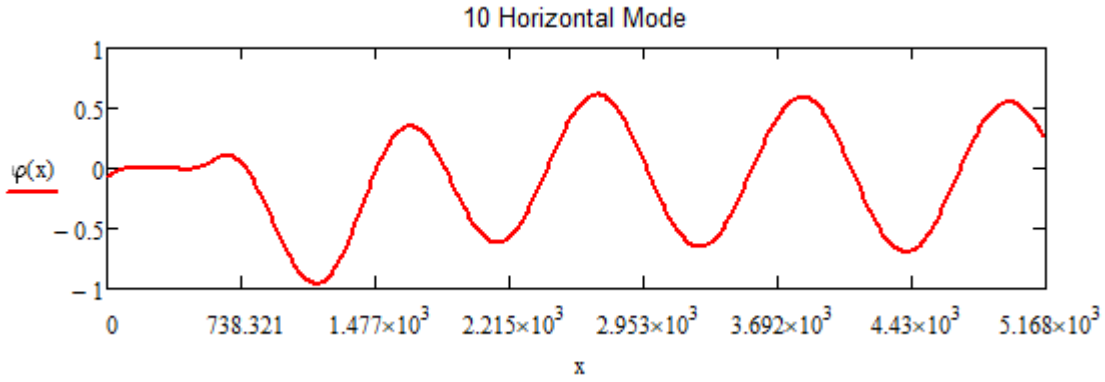

Figure 5.3 Mode shape of the 12th horizontal mode of K11 end anchored bridge.

The maximum modal response σ_y for horizontal wind profiles 1, 2,3 and the specified variations of the turbulence parameters are presented in below.

Table 5.3 Standard deviations of maximum modal responses for horizontal mode 12.

Mode	N400	P10	P50	P90
10. Horizontal n_{10} = 0.1155 Hz	L_u^x = 162 m	L_u^x = 108 m	L_u^x = 232 m	L_u^x = 586 m
	A_u= 6.8	A_u= 3.9	A_u= 7.3	A_u= 16.3
	C_{yu} = 10.0	C_{yu} = 6.4	C_{yu} = 8.0	C_{yu} = 10.8
Wind 1	σ_y = 0.047 m	σ_y = 0.062 m	σ_y = 0.053 m	σ_y = 0.026 m
Wind 2	-	σ_y = 0.048 m	σ_y = 0.036 m	σ_y = 0.019 m
Wind 3	-	σ_y = 0.055 m	σ_y = 0.042 m	σ_y = 0.023 m

5.4 Vertical mode 30

The 30th (across wind) mode is composed of 7½ vertical sinusoidal waves along the bridge line, Figure 5.4. The eigenfrequency and modal mass is obtained from FEM analyses as: n_{30} = 0.1639 Hz and M_{30} = 128676·10^3 kg.

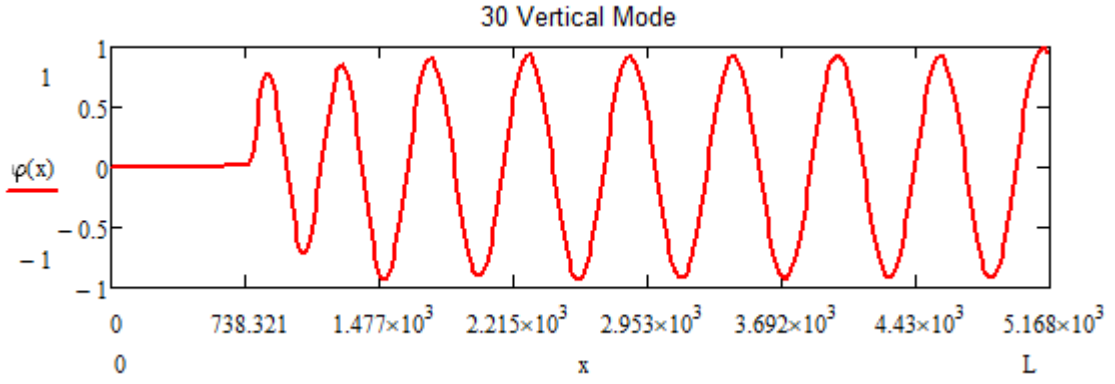

Figure 5.4 Mode shape of 30th mode (vertical) of K11 end anchored bridge.

The maximum vertical modal response σ_z for horizontal wind profiles 1, 2,3 and the specified variations of the turbulence parameters are presented in Table 5.4 below.

Table 5.4 Standard deviations of maximum modal responses for vertical mode 30.

Mode	N400	P10	P50	P90
30. Vertical n_{30} = 0.1639 Hz	L_w^x = 4.2 m	L_w^x = 4.2 m	L_w^x = 4.2 m	L_w^x = 4.2 m
	A_w= 9.4	A_w= 7.7	A_w= 12.3	A_w= 18.2
	C_{yw} = 6.5	C_{yw} = 4.5	C_{yw} = 5.8	C_{yw} = 8.3
Wind 1	σ_z = 0.037 m	σ_z = 0.038 m	σ_z = 0.042 m	σ_z = 0.042 m
Wind 2	-	σ_z = 0.036 m	σ_z = 0.038 m	σ_z = 0.037 m
Wind 3	-	σ_z = 0.037 m	σ_z = 0.04 m	σ_z = 0.039 m

6 Other combinations of turbulence parameters

The conclusion arrived at in section 3 that the largest horizontal responses are obtained from P90 parameters for eigenfrequencies below 0.01 Hz, from P50 parameters for eigenfrequencies in the range 0.01 Hz -0.05 Hz and for P10 parameters for eigenfrequencies above 0.05 Hz is supported by the results presented in Table 5.1,Table 5.2,Table 5.3.

From the Design Basis it is not clear if turbulence parameters are to be combined in such a fashion that length scales, spectral density coefficients and decay parameters are taken from different percentiles to arrive at the most unfavourable turbulent wind loading.

The effect of cross combining the turbulence parameters is investigated below by calculating the spectra of the along wind turbulent wind loading on the bridge line. This investigation is carried out for the along wind horizontal turbulence only as this component displays the largest variations.

6.1 Effect of decay parameter C_{yu}

The influence of the decay parameter is straight forward. Increasing C_{yu} decreases the root coherence and thus the turbulent wind loading as is illustrated in Figure 6.1

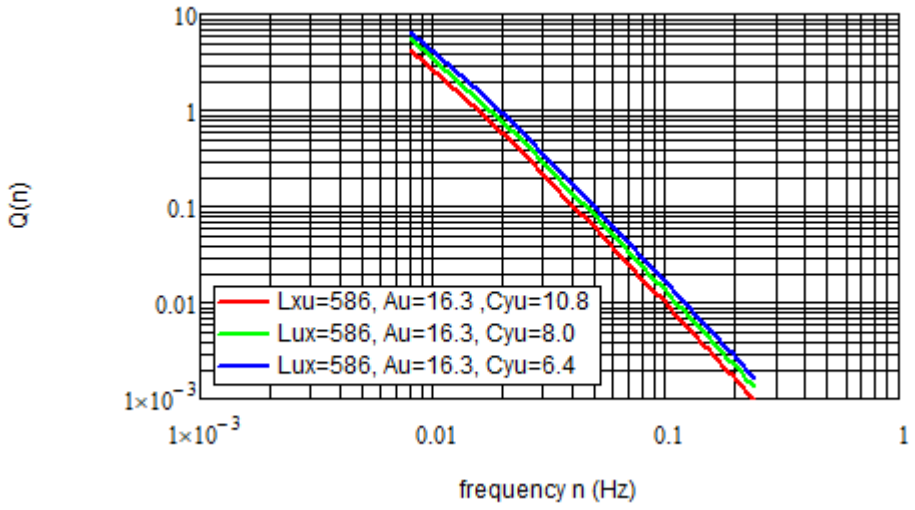

Figure 6.1 Influence of decay parameter on along wind turbulent wind loading on the bridge line.

6.2 Effect of length scale L_u^x and spectral density constant A_u

The length scale and the spectral density constant are interrelated as they both appear as parameters in the power spectrum of the turbulence (3). As is noted from Figure 6.2 the length scale controls the frequency wise position of the intersection between the load spectra and the spectral density constant controls the slope (in a logarithmic plot) of the load spectrum. Thus larger L_u^x moves the loading towards lower frequencies and larger A_u tilts the load spectrum to emphasise lower frequencies over higher frequencies.

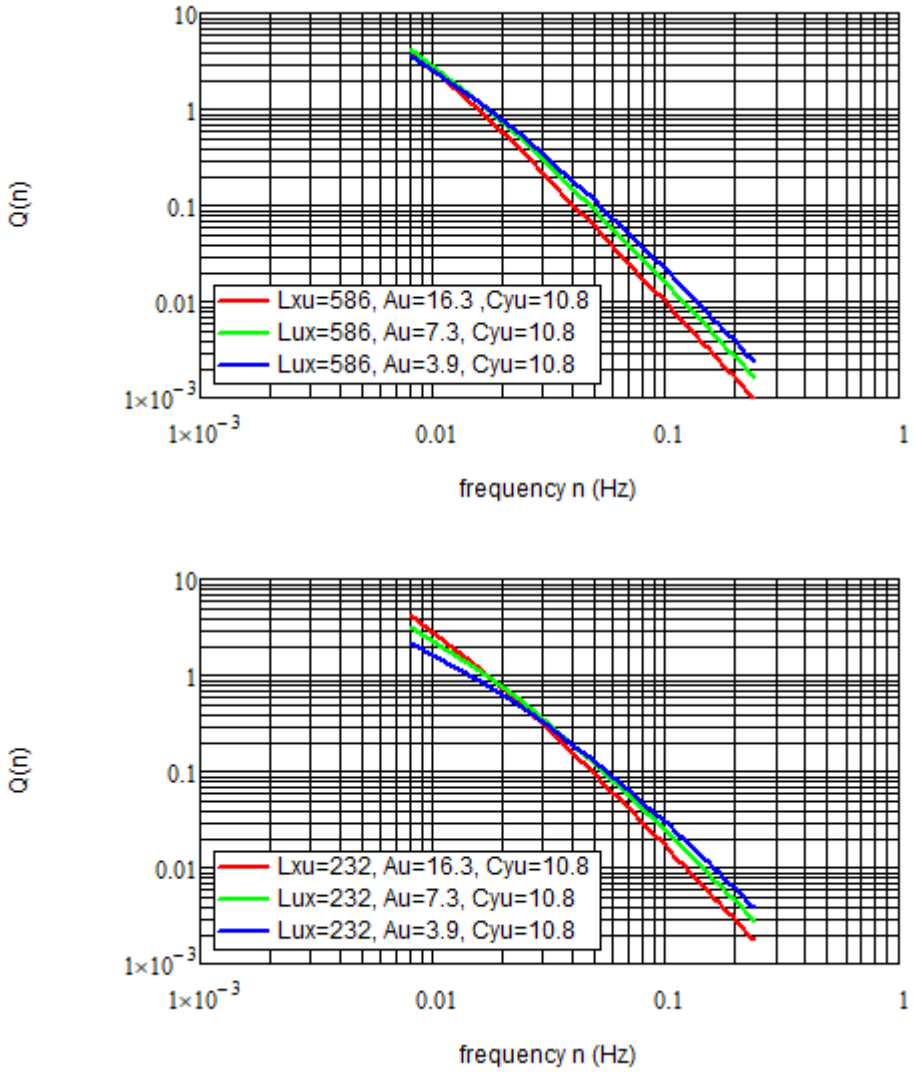

Figure 6.2 Influence of length scale and spectral density constant on along wind turbulent wind loading on the bridge line.

From the above consideration it appears consistent and conservative to adopt the P90 turbulence parameters for the lowest frequencies, the P50 parameters for the mid frequencies and the P10 parameters for the highest frequencies as indicated in the Design Basis, Figure 6.3.

The wind loading at the low and mid frequencies can be increased by adopting a common minimum decay constant C_{yu} = 6.4 for all frequencies, Figure 6.4.

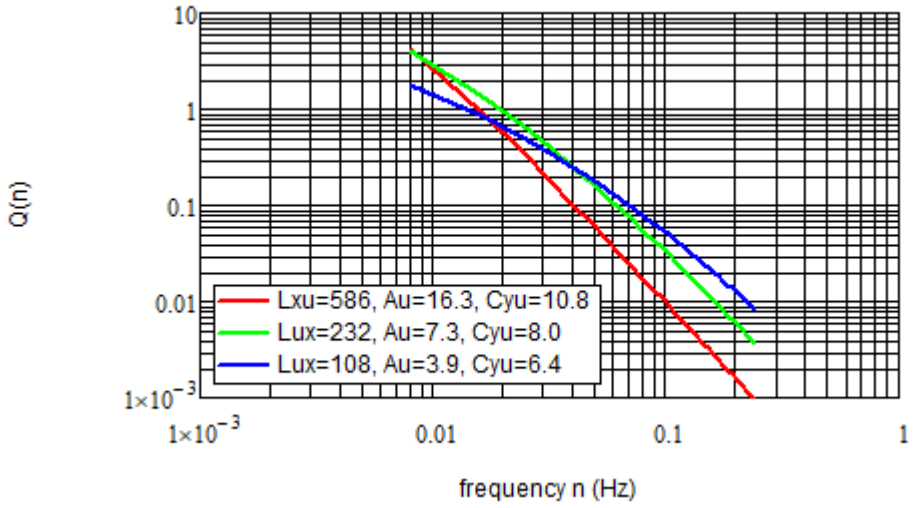

Figure 6.3 Non-dimensional along wind integral turbulent wind loading on the bridge line identical to Figure 3.5. P90 (L_u^x = 586 m ,A_u = 16.3, C_{yu} = 10.8), P50 (L_u^x = 232 m ,A_u = 7.3, C_{yu} = 8.0), P10 (L_u^x = 108 m ,A_u = 3.9, C_{yu} = 6.4).

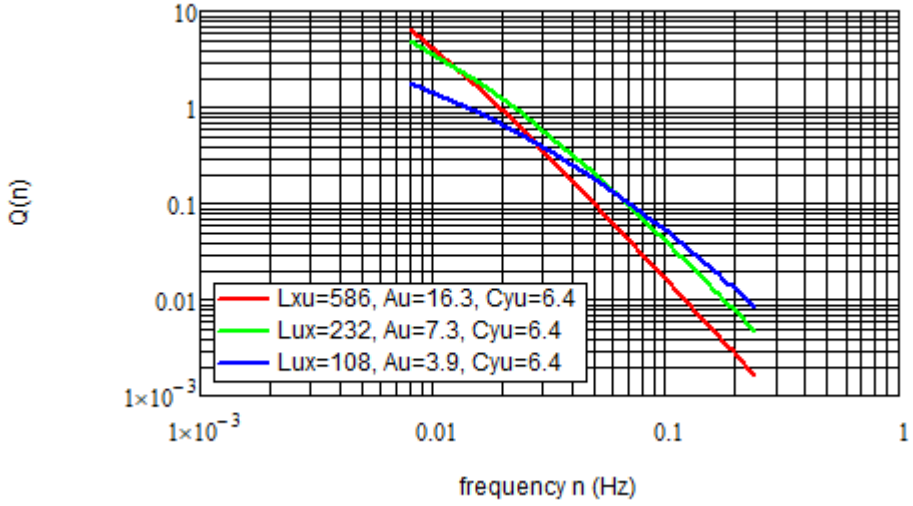

Figure 6.4 Non-dimensional along wind integral turbulent wind loading on the bridge line assuming minimum decay constant for all percentiles.

7 Turbulence parameters for maximum gust response

Section 3.3 concluded that modes having different eigenfrequencies received the largest gust loading for different percentile turbulence properties stated in the Design Basis. While individual treatment of different modes can easily be handled by frequency domain buffeting computations this cannot be achieved in the time domain. Thus it is of interest to investigate if a gust response calculated by using the turbulence properties yielding the maximum gust response for the individual modes can be achieved by picking an appropriate set of turbulence parameters across the percentiles. The numerical example in Table 7.1 below gives the individual and total responses of 9 horizontal modes calculated for three cases:

1. Individual procentiles yielding the maximum response for the individual modes (P90 for mode 1, P50 for modes 2 – 5, P10 for modes 6 – 12).
2. P50 percentile for all modes.
3. L_u^x and A_u from P50, C_{yu} from P10 for all modes.

Table 7.1 Summary of multimode horizontal gust response analysis assuming different turbulence properties.

	Frequency	Modal mass	Mixed percentiles	All P50 percentile	P50: L_u^x, A_u P10: C_{yu}
Mode m	n_m	M_m	σ_y	σ_y	σ_y
1	0.0088 Hz	94828·10^3 kg	P90: 6.53 m	6.16 m	6.41 m
2	0.0166 Hz	54174·10^3 kg	P50: 2.62 m	2.62 m	2.77 m
4	0.0249 Hz	84134·10^3 kg	P50: 0.60 m	0.60 m	0.64 m
5	0.0428 Hz	60714·10^3 kg	P50: 0.34 m	0.34 m	0.38 m
6	0.0599 Hz	67773·10^3 kg	P50: 0.145 m	0.133 m	0.134 m
7	0.0724 Hz	50150·10^3 kg	P10: 0.120 m	0.106 m	0.116 m
8	0.0795 Hz	50487·10^3 kg	P10: 0.098 m	0.084 m	0.099 m
10	0.1155 Hz	34273·10^3 kg	P10: 0.062 m	0.048 m	0.053 m
12	0.1420 Hz	47797·10^3 kg	P10: 0.036 m	0.026 m	0.029 m
$\sqrt{\sum \sigma_{y,m}^2}$	-	-	7.07 m	6.73 m	7.03 m

From Table 7.1 it is noted that it is feasible to arrive at almost the same total response by using the P50 assumption supplemented by the specified P10 coherence as it is for applying the individual percentiles for the modes for which they yield the ultimate response.

8 Conclusions

The general conclusions from the above reported results are summarized as follows:

- Horisontal wind speed profile 1 (constant at fixed height) appear to produce the largest structural responses disregarding mode or response direction. Horizontal wind profile 3 preoduces the second largest responses and wind profile 2 the lowest responses.
- Turbulence parameters corresponding to the different percentile groups (P10, P50, P90) appear to produce larger turbulent loadings in different frequency intervals.
- For the horizontal turbulent loading the P90 percentile produces the largest loading for frequencyies less than 0.01 Hz. The P50 percentile produces the largest loading in the frequency interval 0.01 Hz – 0.035 Hz and the P10 percentile produces the largest loadings at frequencies above 0.035 Hz.
- For the vertical turbulent loading the P90 and P50 percentiles produces roughly equal loadings at frequencies below 0.1 Hz. The P50 percentile produces the largest loadings in the frequency interval 0.1 Hz – 0.35 Hz and the P10 parameters the largest loadings at frequencies above 0.35 Hz
- Application of the length scales and spectral density constants assigned to the different percentiles appear to produce the most conservative gust loadings. Larger loadings for the P50 and P90 percentiles may be obtained by applying the P10 decay constant.
- It appears feasible to approximate maximum total responses, say in time domain gust analyses, by applying the P50 specifications for length scale and spectral density constant supplemented by the P10 specification for the coherence decay constant.

9 References

/1/ MetOcean Design Basis. Document nr.: SBJ-01-C4-SVV-01-BA-001, 14-11-2018.

/2/ N400: Håndbok, Bruprojektering, Statens vegvesen.

/3/ Davenport, A. G.: The prediction of the response of structures to gusty wind, Trondheim, Tapir, 1977.